CHALMERS
UNIVERSITY OF TECHNOLOGY

Analysis of Dual-Motor Drivetrain Architectures with Torque Distribution

Energy Consumption Evaluation for Electric Articulated Haulers

Degree project report in Mobility Engineering

JUNYU ZHAO

DEPARTMENT OF MECHANICS AND MARITIME SCIENCES

CHALMERS UNIVERSITY OF TECHNOLOGY
Gothenburg, Sweden 2026
www.chalmers.se

Degree project report 2026

Analysis of Dual-Motor Drivetrain Architectures with Torque Distribution

Energy Consumption Evaluation for Electric Articulated Haulers

JUNYU ZHAO

CHALMERS
UNIVERSITY OF TECHNOLOGY

Department of MECHANICS AND MARITIME SCIENCES
Chalmers University of Technology
Gothenburg, Sweden 2026

Analysis of Dual-Motor Drivetrain Architectures with Torque Distribution Energy Consumption Evaluation for Electric Articulated Haulers
JUNYU ZHAO

Supervisor: David Berggren, Volvo Construction Equipment
Examiner: Yujing Liu, Department of Electrical Engineering

Degree project report 2026
Department of Mechanics and Maritime Sciences
Chalmers University of Technology
SE-412 96 Gothenburg
Sweden
Telephone +46 31 772 1000

Cover: Volvo A30 Electric articulated hauler

Typeset in LaTeX
Gothenburg, Sweden 2026

Analysis of Dual-Motor Drivetrain Architectures with Torque Distribution Energy Consumption Evaluation for Electric Articulated Haulers
JUNYU ZHAO
Department of Mechanics and Maritime Sciences
Chalmers University of Technology

Abstract

The electrification of heavy-duty articulated vehicles increases the demand for efficient and flexible drivetrain systems. Focusing on the electric articulated hauler platform exemplified by the Volvo A30, this thesis sets out to explore how different dual-motor drivetrain configurations impact the vehicle's energy consumption patterns.

To conduct this investigation, three distinct drivetrain architectures were assessed: a fully coupled baseline design, a partially coupled configuration featuring asymmetric motor sizing with adjusted gear ratios, and a simplified fully decoupled architecture. A unified forward energy flow simulation framework is developed for systematic comparison under representative heavy-duty operating conditions.

The findings of the research highlight that the effectiveness of torque distribution is closely tied to two key factors: operating condition and the drivetrain configuration. Among the investigated configurations, the partially coupled architecture consistently achieves lower energy consumption across all evaluated scenarios. The results suggest that the combination of asymmetric motor sizing, modified gear ratios, and torque distribution strategy can improve drivetrain operating behavior and reduce overall energy consumption under certain load conditions.

In summary, this study provides clear evidence that making moderate system-level adjustments to existing dual-motor drivetrain architectures can unlock potential for improving the energy efficiency of heavy-duty electric articulated vehicles.

Keywords: Dual-motor drivetrain; Heavy-duty electric vehicle; Articulated hauler; Torque distribution; Energy efficiency; Vehicle simulation

Acknowledgements

Looking back, it was a series of unexpected opportunities that brought me to Sweden and to this university. During the past two years, I met many good friends and teachers. I also experienced the development and long-term accumulation of modern European society. At the same time, I gained a deeper understanding of both the current gap between China and Europe and the huge changes China has experienced over the past seventy years.

I feel very fortunate that I was able to find my real interest while studying this field. I was also lucky to witness the rapid growth of China's new energy vehicle industry during this period.

During these two years, the university gave me many opportunities to explore different paths. When I felt uncertain about my future, I still had chances to try different things and learn from them. These experiences helped me better understand what I truly wanted and what kind of work suited me best. I not only learned a lot academically, but also spent more time thinking about my future direction and personal goals in life.

I would also like to thank my teachers for their patience and guidance throughout my studies. Their support helped me continue moving forward during difficult periods. Most importantly, I would like to thank my family. Without their support, I would not have had the chance to grow and develop myself in such an environment.

I also want to thank my girlfriend, who stayed with me during these two years abroad. Even with the long distance between us, she was always there when I felt confused, stressed, or excited, and I always had someone to share my feelings with.

Now, as I prepare to leave Sweden and return to China, I want to set a goal for myself. I hope that in five years and in ten years, we can look back and see how far we have gone. Maybe one day, I can bring the vehicle I worked on back to Europe from China.

Junyu Zhao, Gothenburg, May 2026

List of Acronyms

Below is the list of acronyms that have been used throughout this thesis listed in alphabetical order:

BEV	Battery Electric Vehicle
MPC	Model Predictive Control
PI	Proportional-Integral
SOC	State of Charge
EV	Electric Vehicle

Nomenclature

Below is the nomenclature of indices, sets, parameters, and variables that have been used throughout this thesis.

Indices

i	Gear index
t	Time step index

Parameters

m	Vehicle mass
R	Wheel radius
C_r	Rolling resistance coefficient
θ	Road slope angle
η	Mechanical transmission efficiency
ω_{max}	Maximum motor speed
P_{max}	Maximum motor power
T_{peak}	Peak motor torque
T_{rated}	Rated motor torque
i_g	Gearbox ratio
i_p	Pre-reduction ratio
i_{total}	Total transmission ratio
K_p	Proportional gain of PI controller
K_i	Integral gain of PI controller
α	Torque distribution factor
P_{loss}	Motor power loss
P_{mech}	Mechanical power

P_{elec}	Electrical power
E	Total energy consumption
SOC	Battery state of charge
E_{bat}	Battery energy capacity

Variables

v	Vehicle speed
v_{ref}	Reference vehicle speed
a	Vehicle acceleration
F_{trac}	Traction force
F_{roll}	Rolling resistance force
F_{slope}	Slope resistance force
F_{req}	Required traction force
T_{wheel}	Wheel torque
T_{motor}	Motor torque
T_{big}	Torque of the large motor
T_{small}	Torque of the small motor
ω_{wheel}	Wheel angular speed
ω_{motor}	Motor angular speed
ω_{rear}	Rear motor speed
ω_{front}	Front motor speed
P_{total}	Total electrical power demand
J	Loss minimization objective function

Contents

List of Figures

List of Tables

1

Introduction

1.1 Background: Electrification of Heavy-Duty Articulated Haulers

Articulated haulers are widely used in mining and construction applications for transportation of heavy materials under off-road conditions. These vehicles are required to operate under high load levels for long periods of time, often in harsh environments with varying terrain and ambient conditions. Compared with on-road vehicles, articulated haulers place higher demands on drivetrain robustness, reliability, and lifetime, while efficiency is traditionally not the only design priority.

With the increasing interest in electrification of heavy-duty vehicles, electric drive systems are being considered as alternatives to conventional powertrains for articulated haulers. Electrification offers potential benefits such as high torque capability at low speed, flexible drivetrain architectures, and improved controllability. However, due to the large vehicle mass and demanding duty cycles, the electric drivetrain must be capable of delivering high power continuously while maintaining reliable operation.

In order to meet these requirements, multi-motor drive configurations have been applied in heavy-duty industrial equipment for several decades. In applications such as large grinding mills, dual-motor drive systems have been widely used to achieve high power output by distributing the load between motors [1, 2, 3]. These industrial applications demonstrate that dual-motor configurations are a practical and proven solution for heavy-load and long-term operation.

For articulated haulers, similar requirements exist in terms of power level and operating duration. Therefore, dual-motor electric drive systems can be regarded as a suitable drivetrain architecture for electrified articulated haulers. By distributing the required driving torque between two motors, the system can achieve the demanded performance while maintaining a reasonable level of redundancy and robustness.

However, these systems have shown good performance in high-load applications, but researchers have not fully studied how drivetrain architecture affects system efficiency and energy consumption under heavy-duty conditions. Because of this, more research is needed to study how different dual-motor configurations can improve energy performance.

1.2 Dual-Motor Drive Systems for Articulated Haulers

Figure 1.1: Volvo A30 Electric articulated hauler [24]

This study investigates a dual-motor drive system based on a heavy-duty articulated hauler platform represented by the Volvo A30. This type of vehicle has a high payload capacity. It often operates under medium and high load conditions. The vehicle also works in demanding duty cycles, such as low-speed maneuvering and climbing steep slopes.

The dual-motor drivetrain can be treated as an overactuated system. Different torque distribution solutions can meet the same traction demand. This extra freedom gives more possibilities for performance optimization, especially for energy efficiency.

In the baseline configuration used in this thesis, the system uses two electric motors with the same specifications. The motors work as the main traction units. The motors are installed between the first axle and second axle. A reduction gearbox mechanically connects the motors. The system combines the motor torques and sends them to the vehicle axles.

This type of structure is currently used in the Volvo A30 electric mining truck. I also used this structure as the benchmark for this study. The two motors have identical performance and are mechanically coupled together via gears. The system distributes power evenly between the two motors. This design makes the equipment more stable and simplifies the overall structure. The two motors maintain the same speed, preventing operators from individually adjusting the operating status of each motor according to different working conditions.

Currently, the company has prototypes of a new power transmission structure. Some test vehicles are equipped with three motors, each driving a different axle. This type of equipment is more flexible, allowing operators to individually control the operating status of each motor. This structure makes the vehicle easier to control and reduces power consumption. However, this structure increases the difficulty of equipment assembly and also increases manufacturing costs.

My solution lies between a standard basic structure and a complex multi-motor structure, aiming only to fine-tune the internal structure of the existing equipment.

I want to confirm whether simple modifications can improve energy efficiency while saving money and simplifying the equipment.
This study mainly designs two modification methods. The first method is to replace the motors with motors of different sizes. The second method is to eliminate the mechanical connection between the motors. After these two modifications, the system will have greater flexibility in power allocation. Researchers will carefully control the extent of the modifications to avoid overly complex equipment or increased component costs.
The first modification results in a partially coupled structure. In this structure, the two motors have different pre-reduction ratios and are of different sizes, often a large and a small pair. This structure allows the two motors to rotate independently at different speeds. Torque distribution is more flexible, keeping the motors within their most efficient range.
The second modification results in a completely separate structure. The two motors do not interfere with each other, each driving a different vehicle axle. A simplified model is used here, with a single-stage reduction gear on the front axle and a multi-speed transmission on the rear axle. Although the drivetrain is fully decoupled mechanically, the wheel speeds of the front and rear axles are still generally similar under normal driving conditions. As a result, the motor speeds also maintain a certain relationship during most operating conditions. This approach improves the torque distribution flexibility without significantly increasing construction difficulty or financial investment. Installing multi-speed transmissions throughout the vehicle would further improve flexibility, but this would also significantly increase system cost and complexity, and therefore is not considered in this study.
Different equipment configurations affect motor operation, power consumption, and the overall energy-saving capabilities of the system. Researchers standardized vehicle usage requirements and then compared several different power transmission structures.
The researchers used a baseline structure with the motor connected as a benchmark. Simulation tests were conducted to assess the effectiveness of partially coupled and fully decooupled structures. This allowed them to determine whether simple modifications to the equipment structure could reduce the total power consumption of heavy-duty vehicles during operation.

1.3 Research Objectives and Contributions

Based on the research background and motivation discussed above, this thesis investigates how drivetrain architecture affects the overall performance of dual-motor electric drive systems in articulated haulers.
This research has three main objectives:

1. To establish a unified modeling framework for different dual-motor drivetrain architectures.
2. To analyze the coupling characteristics of the drivetrain structure and study how these characteristics affect motor operating conditions and energy loss distribution.

3. To investigate practical torque distribution strategies enabled by increased drivetrain flexibility, with the goal of improving energy efficiency while maintaining similar vehicle performance.

The main contribution of this thesis is a systematic comparison of different drivetrain architectures. The results show that improving drivetrain flexibility and properly distributing motor torque can create more opportunities for reducing energy consumption.

1.4 Scope and Limitations of the Thesis

This thesis focuses on system-level modeling and performance evaluation of dual-motor electric drive systems for articulated haulers. The study considers different drivetrain architectures with different mechanical coupling characteristics. The study also investigates how these architectures affect efficiency, loss distribution, and energy consumption.

In this thesis, the term "drivetrain architecture" refers to the complete system-level design. The definition includes the mechanical configuration, motor sizing, transmission design, and torque distribution strategy. These elements are closely connected in practical engineering design and together determine system performance.

This work only focuses on torque coordination at the supervisory control level. The study assumes that the inner-loop motor control and inverter dynamics are already properly designed. Therefore, the thesis does not investigate these parts in detail.

To ensure a fair comparison, all drivetrain configurations must satisfy the same vehicle-level performance requirements. These requirements include maximum speed, gradeability, and traction capability. The internal designs, such as motor sizing, gear ratios, and control strategies, are different between configurations. However, all configurations must provide similar overall vehicle performance.

This study has limited detailed motor data. Measured loss maps are only available for the baseline motor. For other motor configurations, the study estimates the loss characteristics by scaling the baseline loss maps and using simplified modeling methods.

These methods are not intended for highly accurate component-level prediction. However, they are suitable for system-level comparison of different drivetrain configurations. Because of this, the conclusions of this study should mainly be understood as relative performance trends instead of exact quantitative results.

This study evaluates performance through simulation under representative articulated hauler operating conditions. The study does not include experimental validation because of limited time and resources. However, the modeling assumptions are based on realistic engineering conditions, so the results can still reflect practical system behavior.

1.5 Literature Review

1.5.1 Development of Dual-Motor Drive Systems

Dual-motor drive systems were first widely applied in heavy industrial machinery, where two motors cooperatively drive a common mechanical load. Typical applications include grinding mills and cement processing equipment, in which dual synchronous motors improve load carrying capability and operational reliability. Early studies mainly focused on the problem of load sharing between coupled motors. Valentine and Scott [1] demonstrated that even small parameter deviations between motors could lead to unequal torque distribution. Subsequent investigations further emphasized the importance of mechanical symmetry and drivetrain structure for maintaining stable operation in practical systems [2, 3, 4, 5].

With the advancement of power electronics and electric drive technology, research attention gradually shifted from purely mechanical coordination toward system-level control. Bouscayrol et al. [6] analyzed multimachine multiconverter systems and showed that coupling topology significantly influences power flow management and system controllability.

Meanwhile, the rapid development of battery electric vehicles (BEVs) accelerated the diversification of electric drivetrain architectures. Emadi et al. [7] reviewed various electric vehicle powertrain configurations and highlighted the growing importance of multi-motor drivetrains. More recently, Wang et al. [8] summarized different dual-motor coupling architectures and showed that drivetrain configuration has a direct impact on efficiency improvement.

Compared with conventional single-motor systems, dual-motor drivetrains introduce additional actuation freedom because multiple torque combinations can satisfy the same traction requirement. This overactuated characteristic enables the drivetrain to optimize objectives beyond simple traction generation, particularly energy efficiency through appropriate torque coordination.

Although dual-motor systems have been extensively studied in passenger vehicles, their application in heavy-duty vehicles remains relatively limited. Articulated haulers continuously operate under high-load conditions, where drivetrain efficiency, durability, and robustness become critical. Under such operating conditions, drivetrain architecture strongly affects motor operating regions and overall system efficiency. However, systematic studies investigating the influence of drivetrain structure on heavy-duty dual-motor energy performance are still insufficient.

1.5.2 From Load Sharing to Torque Allocation

1.5.2.1 Load Sharing in Dual-Motor Systems

In early dual-motor drive applications, the primary coordination objective was load sharing. Since multiple motors simultaneously drive the same load, maintaining balanced torque output is important for preventing overload and ensuring stable operation. As a result, equal torque sharing became a widely adopted engineering solution due to its simplicity and reliability.

Passive Mechanical Coordination

One common approach is passive mechanical coupling, where rigid mechanical connections constrain both motors to operate at the same rotational speed. This structure naturally enables basic load sharing under steady-state conditions and is widely used because of its robust and straightforward implementation. However, the operating states of the motors are strongly constrained by the coupling structure, limiting system flexibility under dynamic operating conditions or parameter variations [6].

Active Electrical Coordination

As electric drive control technologies evolved, active coordination strategies were introduced to improve load sharing performance. Current-following control and power-following control are typical examples. Onwuka and Obe [15] showed that electrical coordination can improve torque balancing accuracy between motors. Nevertheless, many existing approaches still rely on maintaining electrical symmetry among machines, making the system sensitive to parameter mismatches and operating deviations [8].

1.5.2.2 Emergence of Heterogeneous Dual-Motor Systems

Traditional load sharing methods generally assume that the coupled motors possess identical characteristics. Under this assumption, equal torque distribution can simultaneously achieve balanced operation and near-optimal efficiency.

However, modern electric drivetrains increasingly employ heterogeneous motor configurations that combine motors with different power ratings or efficiency characteristics. Such architectures allow each motor to operate within a more suitable efficiency region. Typically, smaller motors are utilized during low-load operation to maintain high efficiency, while larger motors provide the required torque under heavy-load conditions.

In heterogeneous systems, equal torque sharing is no longer necessarily optimal. Instead, torque can be distributed according to the efficiency characteristics of each motor, allowing the drivetrain to better exploit the advantages of different operating regions.

1.5.2.3 Evolution Toward Torque Allocation

Driven by these developments, research focus gradually expanded from traditional load balancing toward energy-oriented torque allocation strategies. Unlike conventional equal-sharing approaches, torque allocation methods determine motor output according to efficiency maps and operating conditions.

By assigning torque based on the performance characteristics of individual motors, the drivetrain can reduce energy losses and improve overall efficiency. This advantage becomes particularly important in heavy-duty applications operating under continuous high-load conditions. Consequently, efficiency-oriented torque allocation has become a key research direction in modern multi-motor electric drivetrains.

1.5.3 Torque Distribution Strategies in Dual-Motor Systems

Torque distribution strategies determine how the total traction demand is shared among motors, directly influencing drivetrain efficiency and energy consumption.

1.5.3.1 Rule-Based Methods

Rule-based strategies allocate torque according to predefined heuristic rules and are widely adopted because of their low implementation complexity.
For systems equipped with identical motors, equal torque distribution remains one of the most commonly used approaches [7]. However, this method implicitly assumes that both motors exhibit similar efficiency characteristics over the entire operating range, which is not always valid in practical applications.
To overcome this limitation, more advanced rule-based methods consider vehicle operating conditions when determining torque allocation. Wang et al. [8] proposed speed- and load-dependent torque split strategies to improve drivetrain efficiency. Similarly, Xu et al. [16] demonstrated that heuristic loss-minimization rules can effectively reduce energy consumption under standard driving cycles.

1.5.3.2 Optimization-Based Methods

Optimization-based methods treat torque allocation as a constrained optimization problem. These methods usually aim to minimize power losses.
Early studies showed that minimizing actuator effort does not always minimize energy consumption. Power-loss-based objectives often provide better performance. Pennycott et al. [21] showed that suitable torque allocation can significantly reduce motor power losses in multi-motor electric vehicles.
Researchers have also widely used control allocation techniques to solve this problem efficiently. Chen and Wang [22] proposed an adaptive energy-efficient control allocation framework for overactuated electric vehicles. Dizqah et al. [23] developed a fast parametric torque distribution method suitable for real-time implementation. These studies also revealed several common trends. For identical motors, single-axle drive is usually more efficient under low torque demand. Equal torque distribution becomes more suitable under high torque demand.
Researchers have also developed more advanced methods with multiple objectives. Li et al. [17] proposed a hierarchical multi-objective framework that balances efficiency and vehicle stability. Researchers have also applied Model Predictive Control (MPC) to handle system constraints and dynamic conditions [11, 18].

1.5.3.3 Influence of Drivetrain Architecture

Drivetrain architecture directly determines the operating region of each motor and the flexibility of torque allocation. Factors such as motor configuration, coupling mechanisms, and transmission ratios strongly affect system efficiency.
Recent studies showed that hardware design and control strategy should be considered together. However, most existing studies focus on passenger vehicles and transient driving cycles. Few studies compare drivetrain architectures under continuous heavy-duty operating conditions.

1.5.3.4 Research Gap

Existing studies have provided many insights into dual-motor powertrains, especially for passenger vehicles and transient driving conditions. However, several limitations still exist for heavy-duty applications.

- Most studies focus on passenger vehicles under transient driving cycles, where load levels are relatively low and highly dynamic.
- Researchers have paid less attention to sustained high-load operation, which is common in heavy-duty articulated haulers.
- Many studies investigate torque distribution strategies, but few studies fully analyze their interaction with drivetrain architecture under continuous high-load conditions.

This research investigates how different dual-motor drivetrain architectures affect torque distribution behavior and energy efficiency under representative heavy-duty operating conditions.

1.5.4 Loss Modeling and Efficiency Characterization of Electrical Machines

Accurate motor loss estimation is important for evaluating energy consumption and designing torque allocation strategies. Existing methods mainly include physics-based thermal models and efficiency-based methods using motor performance characteristics.

1.5.4.1 Thermal Modeling Approaches

Motor losses mainly include copper losses and iron losses [12]. Thermal models predict temperature changes based on these losses and heat transfer mechanisms.
Mellor et al. [14] developed lumped-parameter thermal network models for electrical machines. Staton and Cavagnino [13] improved convection modeling to achieve more accurate temperature prediction. Boglietti et al. [9] highlighted the importance of accurate loss estimation in thermal analysis.
Thermal models provide information about temperature behavior and component limits. However, these models are computationally complex. This limits their use in system-level optimization and real-time control.

1.5.4.2 Efficiency-Based and Scaling Approaches

Efficiency-based methods use torque-speed maps from experiments to describe motor performance. These methods are widely used in vehicle-level energy management, because they are computationally efficient.
Kwon et al. [20] proposed a multi-objective optimization framework for a dual-motor electric vehicle. Their work jointly optimized gear ratios and torque distribution based on motor efficiency characteristics. Their results showed that keeping motors in high-efficiency regions can significantly reduce energy consumption.
Researchers also increasingly use scaling-based methods to generate performance maps for motors with different ratings based on a baseline motor. These methods

allow rapid evaluation of different drivetrain configurations without detailed electromagnetic or thermal redesign.

2

Powertrain Configuration and Parameter Selection

Following the research background and objectives introduced in Chapter 1, this chapter presents the drivetrain architectures investigated in this study together with the related parameter selection process. The main purpose of this chapter is to establish comparable dual-motor drivetrain configurations for the subsequent energy consumption analysis under representative heavy-duty operating conditions.

This study is based on a heavy-duty articulated hauler represented by the Volvo A30 platform. Vehicles of this type usually operate under demanding working conditions and are required to transport heavy payloads over long operating periods. In practical applications, articulated haulers frequently perform low-speed maneuvering, continuous climbing, and operation on uneven terrain. These working conditions place high demands on the drivetrain system in terms of traction capability, robustness, thermal loading, and overall energy efficiency.

Compared with conventional passenger vehicles, heavy-duty articulated haulers operate under higher sustained load levels and more severe duty cycles. Therefore, the drivetrain architecture not only affects vehicle performance, but also strongly influences motor operating regions, transmission behavior, and overall system energy consumption. Because of this, the selection of drivetrain configuration and transmission parameters becomes particularly important for heavy-duty electric vehicles.

To ensure a meaningful and fair comparison, all drivetrain configurations investigated in this study are designed to satisfy the same vehicle-level performance targets. These targets include maximum vehicle speed, gradeability, and traction capability. Although the investigated architectures differ in motor sizing, transmission layout, coupling characteristics, and torque distribution flexibility, each configuration must still provide equivalent overall vehicle performance under the same operating conditions.

Based on these common performance requirements, the following sections introduce the fully coupled, partially coupled, and fully decoupled drivetrain architectures. The chapter also presents the related transmission parameter design process, gear ratio selection, and shift strategy development for each configuration.

2.1 Overview of Powertrain Architectures

2.1.1 Fully Coupled Architecture

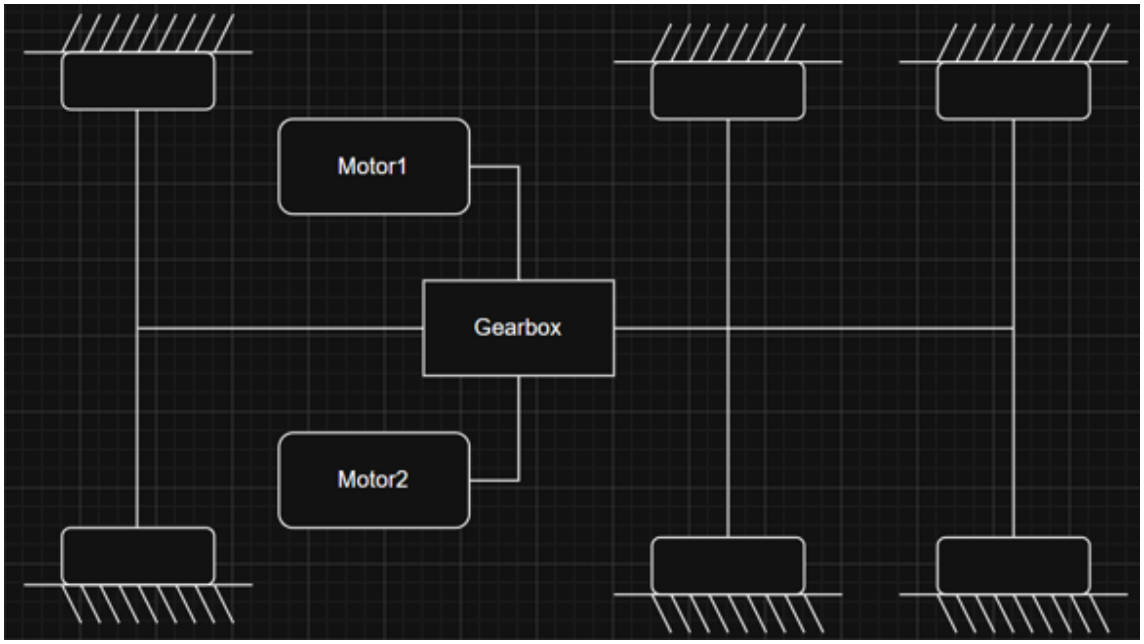

Figure 2.1: Fully Coupled Architecture

In the fully coupled architecture, the system uses two electric motors with identical specifications. A common gearbox mechanically connects the two motors. Because of this connection, both motors always operate at the same rotational speed:

$$\omega_1 = \omega_2 \tag{2.1}$$

The gearbox combines the torque produced by the two motors and transmits it to the drivetrain. Since the motors have identical characteristics and rigid mechanical coupling, the system usually distributes torque equally or close to equally under normal operating conditions.

This configuration represents a traditional dual-motor drivetrain. The architecture has a simple structure, high robustness, and easy implementation. However, the strong mechanical constraint limits the flexibility of torque allocation and operating point selection. Since both motors always rotate at the same speed, the system cannot independently place the motors in their high-efficiency regions. This limitation may reduce overall system efficiency under different load conditions.

Because of this, this study uses the fully coupled architecture as the baseline configuration for comparison with more flexible drivetrain architectures.

2.1.2 Partially Coupled Architecture

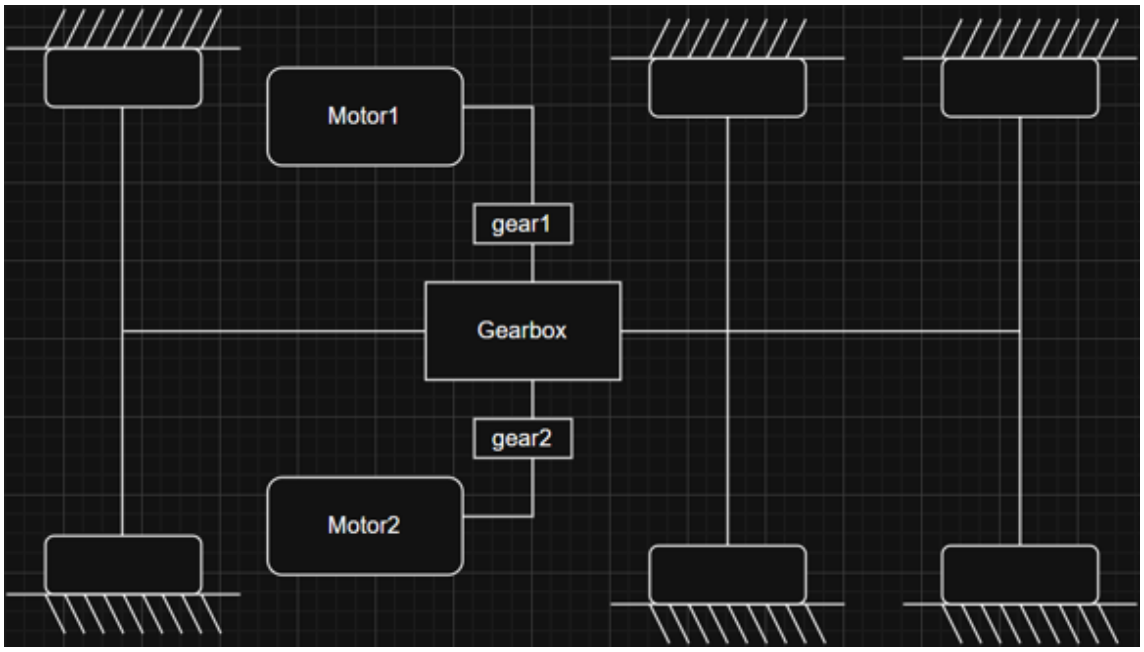

Figure 2.2: Partially Coupled Architecture

In the partially coupled architecture, the system adds additional pre-reduction stages between each motor and the main gearbox. The two motors use different specifications. The system typically uses one larger motor and one smaller motor. The motors connect to the drivetrain through different reduction ratios.

Because of this design, the rotational speeds of the two motors are no longer the same:

$$\omega_1 \neq \omega_2 \tag{2.2}$$

However, the motors are still mechanically connected through the common gearbox. The system still combines the motor torques before transmitting them to the wheels.

This configuration relaxes the strict speed constraint found in the fully coupled architecture. The system gains an additional degree of freedom for operating point selection. Since the motors can operate at different speeds, the system can better match the efficiency characteristics of each motor, especially when the motors have different power ratings.

At the same time, the partially coupled architecture keeps a relatively simple mechanical structure compared with fully decoupled systems. Because of this, the architecture provides a balance between flexibility and system complexity. The system can achieve better efficiency optimization potential without greatly increasing hardware requirements.

2.1.3 Fully Decoupled Architecture

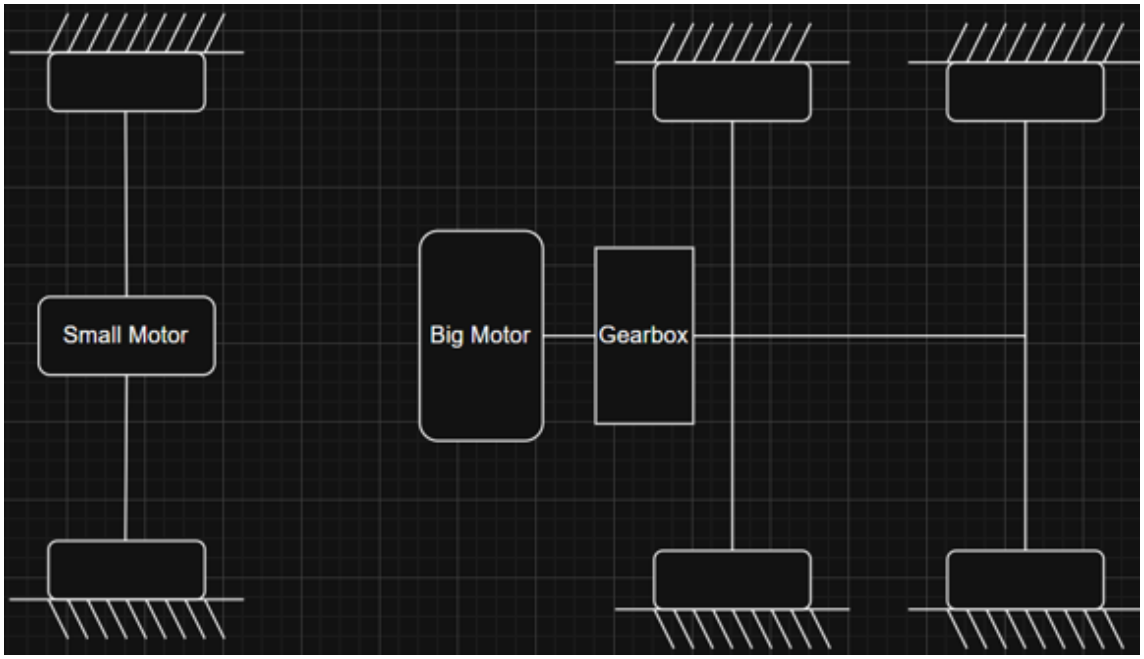

Figure 2.3: Fully decoupled Architecture

In the fully decoupled architecture, the two motors are no longer mechanically connected through a common drivetrain. Instead, each motor independently drives a different axle of the vehicle. In most cases, one motor drives the front axle and the other motor drives the rear axle.

In this configuration, the system can independently control both motor speed and motor torque:

$$\omega_1 \neq \omega_2 \tag{2.3}$$

This complete decoupling removes the mechanical constraints between the motors. The system gains the highest level of freedom for torque distribution and operating point selection. Because of this flexibility, the system can apply advanced control strategies based on efficiency, load conditions, or other performance objectives.

The fully decoupled architecture allows each motor to operate closer to its optimal efficiency region over a wide operating range. However, this higher flexibility also increases system complexity. The system requires more hardware components, more advanced control strategies, and better coordination between axles.

Overall, this architecture is the most flexible distributed drive configuration investigated in this study. The architecture also provides a reference for evaluating the potential benefits of fully independent motor operation.

2.2 Gear Ratio Determination Based on Performance Benchmarks

Since the transmission configuration of the electric version of the Volvo A30 articulated hauler is not publicly available, the gear ratios of the fully coupled electric architecture are derived from dynamic performance targets inferred from the diesel-powered reference vehicle.
The following performance benchmarks are adopted:

- Maximum vehicle speed: approximately $56 km/h$
- Launch gradeability: 45% at 1 km/h (full load)

The baseline vehicle parameters are summarized in Table 2.1.

Table 2.1: Baseline vehicle parameters

Parameter	Value
Vehicle mass m	55,000 kg
Wheel radius R	0.81 m
Peak motor torque (per motor) T_{peak}	440 Nm
Number of motors	2
Maximum motor speed n_{max}	10,000 rpm
Maximum motor power (per motor)	200 kW
Mechanical efficiency η	0.89
Rolling resistance coefficient C_r	0.03

Aerodynamic drag is neglected in climbing conditions due to the relatively low operating speeds.

Third Gear Ratio from Maximum Vehicle Speed

The third gear ratio is determined from the maximum vehicle speed constraint:

$$i_{g3} = \frac{n_{max} \cdot 2\pi R}{60 \cdot v_{max}} \tag{2.4}$$

The resulting value is summarized in Table 2.2.

First Gear Ratio from Launch Gradeability

The required tractive force under grade conditions is given by

$$F_{req} = mg \sin\theta + C_r mg \tag{2.5}$$

The corresponding wheel torque requirement is

$$T_{wheel} = F_{req} \cdot R \tag{2.6}$$

The wheel torque provided by the drivetrain is

$$T_{wheel} = 2 \cdot T_{peak} \cdot i \cdot \eta \tag{2.7}$$

By equating the required and available torque, the first gear ratio can be determined. The resulting value is summarized in Table 2.2.

Second Gear Ratio

The intermediate gear ratio is selected using geometric progression:

$$i_{g2} = \sqrt{i_{g1} \cdot i_{g3}} \tag{2.8}$$

The resulting value is summarized in Table 2.2.

Verification of Sustained Gradeability

The required wheel power under sustained grade conditions is

$$P_{wheel} = F_{req} \cdot v \tag{2.9}$$

The corresponding motor power is

$$P_{motor} = \frac{P_{wheel}}{\eta} \tag{2.10}$$

The available motor power is

$$P_{available} = 2 \cdot P_{peak} \tag{2.11}$$

The calculated results confirm that the sustained gradeability requirement is satisfied.

Final Gear Ratios

The final gear ratios are summarized in Table 2.2.

Table 2.2: Gear ratios for the fully coupled architecture

Gear	Ratio
First gear (i_{g1})	246
Second gear (i_{g2})	115
Third gear (i_{g3})	54

These gear ratios satisfy all defined performance benchmarks and establish the reference configuration for subsequent comparison with alternative drivetrain architectures.

2.3 Partially Coupled Architecture Drivetrain Design

The partially coupled architecture uses different pre-reduction stages for the two motors. This design allows the motors to operate at different rotational speeds, even though motors are still mechanically connected.

$$i_{total} = i_p \cdot i_g \tag{2.12}$$

where i_p is the pre-reduction ratio and i_g is the gearbox ratio.
This study keeps the same vehicle parameters and dynamic performance targets to ensure a fair comparison.

Motor Power Allocation

The partially coupled architecture uses an asymmetric motor sizing strategy. The system uses a larger motor to provide most of the traction demand. A smaller motor provides additional support.
Based on the design considerations introduced above, this study selects a power split of 75% for the big motor and 25% for the small motor.
The resulting motor ratings are summarized in Table 2.3.

Table 2.3: Motor parameters for the partially coupled architecture

Parameter	Primary motor	Secondary motor
Rated power	300 kW	100 kW
Peak torque	660 Nm	220 Nm
Pre-reduction ratio i_p	1.3	1.6

Third Gear Ratio from Maximum Vehicle Speed

In the partially coupled architecture, the small motor operates at a higher rotational speed, because it has larger pre-reduction ratio. Therefore, the maximum speed constraint is governed by the small motor.
The motor speed is given by

$$\omega_m = \omega_w \cdot i_g \cdot i_p \tag{2.13}$$

To satisfy the motor speed limit, the following condition must be fulfilled:

$$i_{g3} \cdot i_{p,small} \leq \frac{\omega_{max}}{\omega_w} \tag{2.14}$$

The resulting third gear ratio is summarized in Table 2.4.

First Gear Ratio from Launch Gradeability

The first gear ratio is determined by the launch gradeability requirement and remains unchanged compared to the baseline configuration. This ensures that the required wheel torque can still be achieved and that climbing performance is preserved.
The resulting value is summarized in Table 2.4.

Second Gear Ratio

The intermediate gear ratio is selected using geometric progression:

$$i_{g2} = \sqrt{i_{g1} \cdot i_{g3}} \tag{2.15}$$

The resulting value is summarized in Table 2.4.

Final Gear Ratios

The final gearbox ratios of the partially coupled architecture are summarized in Table 2.4.

Table 2.4: Gear ratios for the partially coupled architecture

Gear	Ratio
First gear (i_{g1})	179
Second gear (i_{g2})	77
Third gear (i_{g3})	33

With this configuration, the maximum vehicle speed can be achieved without exceeding the small motor speed limit. At the same time, the first gear ratio remains unchanged, ensuring that the original launch gradeability is preserved. The use of geometric progression maintains a balanced distribution between gear ratios, supporting smooth shifting behavior and stable drivetrain performance.

2.4 Fully Decoupled Architecture Drivetrain Design

The fully decoupled architecture adopts a distributed configuration in which the front and rear axles are driven by independent electric motors. In contrast to the previous configurations, the front axle employs a single-speed reduction, while the rear axle retains a three-speed gearbox. This configuration allows the rear axle to provide high torque capability during low-speed operation while maintaining efficient operation at higher vehicle speeds.
To ensure a fair comparison with the previous architectures, the same vehicle parameters and dynamic performance benchmarks are maintained.

Motor Power Allocation

Due to the load distribution characteristics of articulated haulers, a larger portion of the traction demand is carried by the rear axle, particularly under climbing conditions. Therefore, a power allocation of 75% to the rear axle and 25% to the front axle is adopted.
The resulting motor parameters are summarized in Table 2.5.

Table 2.5: Motor parameters for the fully decoupled architecture

Parameter	Rear motor	Front motor
Rated power	300 kW	100 kW
Peak torque	660 Nm	220 Nm

Front Axle Reduction Ratio

The front axle adopts a single-speed reduction. To ensure that the motor operates within the allowable speed range across the full vehicle speed domain, the reduction ratio is selected based on the maximum vehicle speed constraint.

To maintain consistency and avoid excessive motor speed, the front axle ratio is aligned with the highest gear ratio of the rear axle. The resulting value is summarized in Table 2.6.

This selection ensures speed compatibility but limits the torque contribution capability of the front motor. As a result, the front motor primarily acts as an auxiliary power source under moderate load conditions.

Rear Gearbox Ratios

Due to the reduced torque contribution from the front axle, the rear axle is required to provide the majority of the traction demand, especially under high-load conditions. Therefore, the rear gearbox ratios are determined based on the required wheel torque.

The total wheel torque can be expressed as

$$T_{wheel} = T_{rear,peak} \cdot i_{rear} \cdot \eta + T_{front,peak} \cdot i_{front} \cdot \eta \tag{2.16}$$

By equating the required wheel torque with the available torque, the first gear ratio of the rear axle can be determined.

The third gear ratio is selected based on the maximum vehicle speed constraint, ensuring that the rear motor does not exceed its allowable speed.

The intermediate gear ratio is determined using geometric progression:

$$i_{rear,2} = \sqrt{i_{rear,1} \cdot i_{rear,3}} \tag{2.17}$$

The resulting values are summarized in Table 2.6.

Final Transmission Ratios

The final transmission ratios of the fully decoupled architecture are summarized in Table 2.6.

Table 2.6: Transmission ratios for the fully decoupled architecture

Component	Ratio
Front axle (i_{front})	54
Rear gear 1 ($i_{rear,1}$)	309
Rear gear 2 ($i_{rear,2}$)	129
Rear gear 3 ($i_{rear,3}$)	54

2.5 Gear Shift Strategy

To ensure a fair and consistent comparison between the three drivetrain architectures, a unified gear shift strategy is adopted. The gear shifting strategy uses motor speed instead of vehicle speed as the shifting condition. This helps different drivetrain configurations operate in similar motor efficiency ranges.
The main objectives of the shift strategy are:

- Avoid motor overspeed
- Keep the motors operating in efficient regions
- Maintain sufficient traction torque after shifting
- Ensure consistent operating conditions across different architectures

Motor Speed Constraint

The upshift condition is determined based on motor speed:

$$\omega_{shift} = k \cdot \omega_{max} \tag{2.18}$$

where k is the shift factor. In this study, $k = 0.9$, meaning that gear shifting occurs when the motor speed reaches 90% of the maximum motor speed. This margin helps prevent motor overspeed during shifting.

Motor Speed and Vehicle Speed Relationship

The motor speed is related to the wheel speed through the transmission ratio:

$$\omega_m = \omega_w \cdot i_{total} \tag{2.19}$$

$$\omega_w = \frac{v}{R} \tag{2.20}$$

2.5.1 Fully Coupled Architecture

Since both motors are mechanically coupled, they operate at identical speeds. The shift points are determined based on the motor speed constraint:

$$\omega_m = \omega_{shift} \tag{2.21}$$

The wheel speed thresholds are given by

$$\omega_w = \frac{\omega_{shift}}{i_g} \tag{2.22}$$

The post-shift motor speed is determined by the ratio change:

$$\omega_{after} = \omega_{shift} \cdot \frac{i_{next}}{i_{current}} \tag{2.23}$$

The resulting shift characteristics are summarized in Table 2.7.

Table 2.7: Shift characteristics for fully coupled architecture

Shift	ω_w (rad/s)	ω_{after} (rad/s)
$1 \rightarrow 2$	3.8	443
$2 \rightarrow 3$	8.2	439

2.5.2 Partially Coupled Architecture

In the partially coupled architecture, the motors operate at different speeds due to distinct pre-reduction ratios. The motor speed is given by

$$\omega_m = \omega_w \cdot i_g \cdot i_p \tag{2.24}$$

The wheel speed threshold is defined as

$$\omega_w = \frac{\omega_{shift}}{i_g \cdot i_{p,limiting}} \tag{2.25}$$

The post-shift motor speed is

$$\omega_{after} = \omega_{shift} \cdot \frac{i_{next}}{i_{current}} \tag{2.26}$$

The resulting shift characteristics are summarized in Table 2.8.

Table 2.8: Shift characteristics for partially coupled architecture

Shift	ω_w (rad/s)	$\omega_{after,big}$ (rad/s)	$\omega_{after,small}$ (rad/s)
$1 \rightarrow 2$	3.3	330	406
$2 \rightarrow 3$	7.7	328	404

2.5.3 Fully Decoupled Architecture

In the fully decoupled architecture, only the rear motor participates in gear shifting, while the front motor operates with a fixed reduction ratio.
The shift condition is defined as

$$\omega_m = \omega_{shift} \tag{2.27}$$

Thus, the wheel speed thresholds are

$$\omega_w = \frac{\omega_{shift}}{i_{rear}} \tag{2.28}$$

The post-shift motor speed is

$$\omega_{after} = \omega_{shift} \cdot \frac{i_{next}}{i_{current}} \tag{2.29}$$

The resulting shift characteristics are summarized in Table 2.9.

Table 2.9: Shift characteristics for fully decoupled architecture

Shift	ω_w (rad/s)	ω_{after} (rad/s)
$1 \rightarrow 2$	3.0	393
$2 \rightarrow 3$	7.3	394

2.5.4 Upshift Strategy

The upshift thresholds are summarized in Table 2.10.

Architecture	1→2 (rad/s)	2→3 (rad/s)
Fully Coupled	3.8	8.2
Partially Coupled	3.3	7.7
Fully Decoupled	3.0	7.3

Table 2.10: Upshift thresholds for different architectures

2.5.5 Downshift Strategy

To prevent frequent gear oscillations during transient operating conditions, a hysteresis band is introduced between upshift and downshift thresholds

$$\omega_{down} < \omega_{up} \tag{2.30}$$

In this study, the downshift thresholds are selected as approximately 80% of the corresponding upshift values, ensuring stable gear transitions while maintaining sufficient traction capability.
The resulting downshift thresholds are summarized in Table 2.11.

Architecture	2→1 (rad/s)	3→2 (rad/s)
Fully Coupled	3.0	6.6
Partially Coupled	2.6	6.2
Fully Decoupled	2.4	5.8

Table 2.11: Downshift thresholds for different architectures

2.6 Summary

This chapter presented the drivetrain configurations investigated in this study, including the fully coupled, partially coupled, and fully decoupled dual-motor architectures. Although the three configurations differ in terms of drivetrain topology, motor sizing, transmission layout, and torque distribution flexibility, all architectures were designed to satisfy equivalent vehicle-level performance requirements.
Based on these common performance targets, the corresponding transmission ratios and shift strategies were determined for each architecture. The proposed shift strategy ensures that all motors operate below their allowable speed limits while maintaining operation within relatively efficient operating regions. By defining the shift behavior based on motor speed, the three drivetrain architectures are subjected to comparable operating conditions throughout the driving cycle.
As a result, the subsequent differences observed in motor operating behavior and energy consumption can be primarily associated with drivetrain configuration and torque distribution characteristics rather than inconsistencies in vehicle capability or shift control strategy.
Overall, the investigated drivetrain configurations represent different levels of mechanical coupling and operating flexibility, providing the basis for the unified modeling framework and comparative energy consumption analysis presented in the following chapter.

3

Modeling of Powertrain and Energy Consumption Optimization

Following the drivetrain configurations developed in the previous chapter, this chapter presents the modeling framework used for the comparative energy consumption analysis. Since the investigated architectures differ in drivetrain topology, transmission configuration, and motor operating characteristics, a consistent system-level model is required to ensure a fair comparison under identical operating conditions.
The developed framework follows a forward energy flow approach, starting from vehicle longitudinal dynamics and extending to drivetrain transmission behavior, torque distribution, motor loss evaluation, and energy accumulation. Although the three drivetrain architectures differ in structural configuration, the same overall modeling methodology is applied to all cases in order to maintain consistent evaluation conditions.
Particular attention is given to how drivetrain configuration influences motor operating points and overall energy consumption throughout the driving cycle. Therefore, the modeling approach is designed not only to capture vehicle-level performance, but also to reflect the interaction between transmission characteristics, torque distribution behavior, and motor efficiency.
Based on this framework, the following sections introduce the individual modeling modules.

3.1 Overall Modeling Framework

The corresponding forward energy flow and module interaction within the unified modeling framework are summarized in Fig. 3.1. To ensure a fair and systematic comparison, this study establishes a unified modeling framework for all three dual-motor architectures. Each drivetrain architecture is evaluated together with its related design choices, including motor sizing, transmission configuration, and torque distribution strategy. This study does not treat these elements as separate variables. Instead, the study considers them as integrated parts of each architecture to reflect realistic system-level design.
The overall modeling process follows a forward energy flow from vehicle-level dynamics to component-level loss calculation.
The simulation starts from the prescribed driving cycle. The vehicle longitudinal

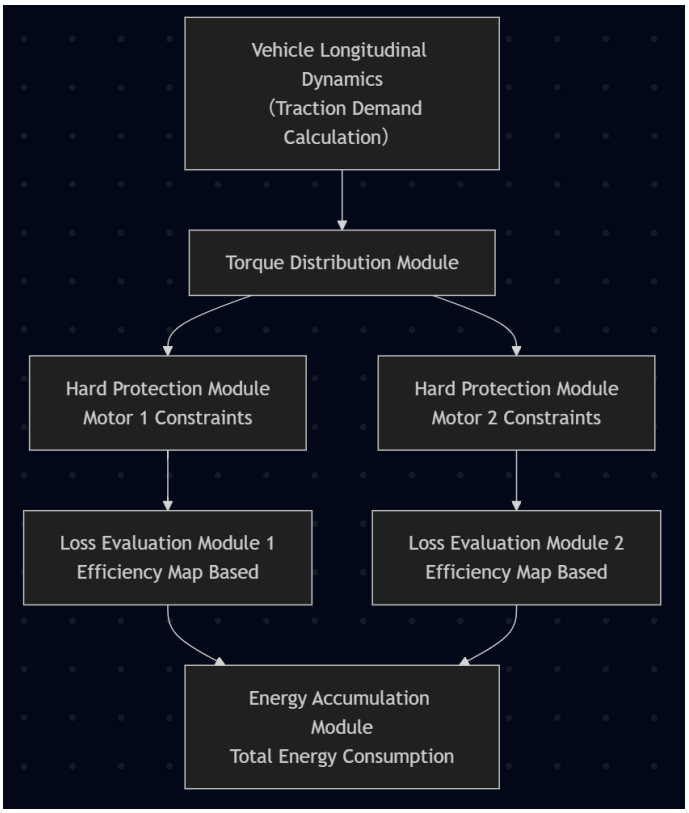

Figure 3.1: Forward Energy Flow Modeling Framework

dynamics model calculates the required traction force based on rolling resistance and road slope. These factors represent the external resistance acting on the vehicle, and the model includes them in the traction demand calculation.

The system then calculates the required wheel torque and wheel speed. The transmission system converts these values into motor-side quantities according to the selected gear ratio. After this step, the torque allocation module distributes the total torque demand between the two motors based on the selected drivetrain configuration.

To ensure physically feasible operation, the model includes a constraint module. This module limits the requested torque within allowable operating boundaries. The module prevents the motors from exceeding temperature limits, maximum torque limits, and maximum power capability.

The motor operating condition is determined by motor torque and motor speed. These operating points are sent to the loss calculation module. In this study, motor losses are estimated using efficiency maps, which describe efficiency characteristics under different operating conditions. Transmission losses are also included through a constant mechanical efficiency.

The electrical power consumption is then integrated to obtain the total vehicle energy consumption.

The total energy consumption considered in this study mainly includes:

- Motor losses based on efficiency maps,
- Transmission losses represented by mechanical efficiency,

- Resistance-related power caused by rolling resistance and road gradient.

Other energy losses, such as battery internal losses and auxiliary power consumption, are not included in the model. The main purpose of this study is to compare the effects of drivetrain architecture and torque distribution strategies on motor-related energy consumption. Since all configurations use the same vehicle parameters and driving conditions, these neglected losses are assumed to be similar in all cases and therefore do not influence the relative comparison results.
This modeling framework ensures that the differences in energy consumption observed in the results can be directly attributed to the variations in drivetrain architecture and control strategy.

3.2 Vehicle Longitudinal Dynamics

The longitudinal dynamics of the electric hauler are modeled based on force equilibrium. The traction force generated by the powertrain is used to overcome resistive forces and accelerate the vehicle:

$$ma = F_{trac} - F_{roll} - F_{slope} \tag{3.1}$$

where the rolling resistance and slope resistance are given by:

$$F_{roll} = C_r mg \tag{3.2}$$

$$F_{slope} = mg \sin\theta \tag{3.3}$$

Thus, the vehicle acceleration can be expressed as:

$$a = \frac{F_{trac} - C_r mg - mg \sin\theta}{m} \tag{3.4}$$

To track the reference driving cycle, a PI controller is employed to generate the required traction force based on the speed error:

$$e = v_{ref} - v \tag{3.5}$$

$$F_{req} = K_p e + K_i \int e dt \tag{3.6}$$

The gearbox module determines the active transmission ratio i_{total} based on the current wheel speed, ensuring that the motor operates within an appropriate speed range.
For the fully coupled architecture (Model 1), both motors are mechanically coupled to the same drivetrain and therefore operate at identical rotational speeds. The motor speed is calculated as:

$$\omega_{\text{motor}} = i_{total} \cdot \omega_{\text{wheel}} \tag{3.7}$$

For the partially coupled architecture (Model 2), each motor connects to the drivetrain through an additional pre-reduction stage. Because of this design, the two

motors no longer operate at the same rotational speed. The system calculates the motor speeds separately:

$$\omega_{\text{motor},1} = i_{total} \cdot i_{p,1} \cdot \omega_{\text{wheel}} \tag{3.8}$$

$$\omega_{\text{motor},2} = i_{total} \cdot i_{p,2} \cdot \omega_{\text{wheel}} \tag{3.9}$$

where $i_{p,1}$ and $i_{p,2}$ represent the pre-reduction ratios of the two motors.
For the fully decoupled architecture (Model 3), the two motors drive different axles. Therefore, the system uses independent transmission paths for the two motors. The rear axle, driven by the larger motor, is equipped with a multi-speed gearbox, while the front axle, driven by the smaller motor, uses a single-stage fixed reduction.
The motor speeds are thus calculated as:

$$\omega_{\text{rear}} = i_{rear} \cdot \omega_{\text{wheel,rear}} \tag{3.10}$$

$$\omega_{\text{front}} = i_{front} \cdot \omega_{\text{wheel,front}} \tag{3.11}$$

where i_{rear} is the gear ratio selected by the gearbox on the rear axle, and i_{front} is the fixed reduction ratio of the front axle.
The requested traction force is further limited by a constraint module to ensure that the powertrain operates within its physical limits, resulting in the actual traction force F_{trac} applied to the vehicle.
The required wheel torque is obtained from the traction force:

$$T_{wheel} = F_{trac} \cdot R \tag{3.12}$$

which is then converted to motor-side torque considering the transmission ratio and mechanical efficiency:

$$T_{motor} = \frac{T_{wheel}}{i_{total} \cdot \eta_{mech}} \tag{3.13}$$

These motor operating points, defined by torque and speed, are used for subsequent loss evaluation and energy consumption analysis.
For the partially coupled and fully decoupled architectures, the same modeling framework is applied. However, due to differences in transmission topology and gear ratios, the motor speeds and torque distributions differ, resulting in distinct operating points for each motor.

3.3 Energy Consumption Optimization with Torque Distribution

In order to determine how the total traction demand is allocated between the two motors, different torque distribution strategies are adopted for the three architectures.

3.3.1 Baseline Equal Torque Distribution Strategy

For the fully coupled architecture, the two motors have identical specifications and operate under the same rotational speed due to mechanical coupling. A simple and robust torque distribution strategy is adopted, where the total motor torque is equally shared between the two machines, as this represents the most efficient torque allocation under the imposed mechanical coupling constraint.

$$T_1 = T_2 = \frac{T_{motor,total}}{2} \tag{3.14}$$

In addition, the system applies torque limits and power limits to ensure that the motor operating points remain within the allowable operating region. This equal torque distribution strategy works as a baseline reference for comparison with more advanced methods.

3.3.2 Optimization-Oriented Torque Distribution Strategy

For the partially coupled and fully decoupled architectures, the two motors have different sizes and operating characteristics. Because of this difference, equal torque distribution is no longer the optimal solution. Therefore, this study uses an efficiency-oriented torque distribution strategy.
The system distributes the total motor torque demand between the two motors using a scalar allocation factor $\alpha \in [0, 1]$:

$$T_{big} = \alpha \cdot T_{motor,total} \tag{3.15}$$

$$T_{small} = (1 - \alpha) \cdot T_{motor,total} \tag{3.16}$$

The controller performs a discrete search over α within a predefined range to find the optimal torque split. For each candidate value of α, the system performs the following steps:

- The system calculates the corresponding motor torques while maintaining the required total traction demand.
- The system checks the torque limits of both motors to ensure feasible operation.
- The system applies instantaneous power limits to prevent the motors from exceeding their rated capabilities.
- The system maps the motor operating points onto efficiency maps to calculate the corresponding power losses.

The system then calculates the total loss as the sum of the losses of both motors:

$$J = P_{loss,big} + P_{loss,small} \tag{3.17}$$

The system selects the value of α that minimizes the total loss. This value becomes the optimal torque distribution.
To improve numerical robustness and reduce large torque fluctuations, the controller also applies additional smoothing and constraint methods. The controller limits the

range of α, introduces a dead-zone to suppress small variations, and uses a first-order filter to ensure smooth changes in torque allocation.
In addition, the controller checks whether the final torque allocation can satisfy the required traction demand after applying motor constraints. If the combined wheel-side torque cannot meet the requested traction demand, the controller recalculates the torque distribution within the feasible operating region until the system obtains a valid solution.
This strategy allows the motors to operate at different operating points and better utilize their efficiency characteristics. As a result, the system has the potential to reduce energy consumption compared with equal torque distribution.

3.4 Hard Protection Module

To ensure safe and physically feasible operation of the electric machines, a hard protection module is implemented in all architectures. This module limits the commanded motor torque based on both power and thermal constraints.
First, a power-based torque limit is applied. The maximum allowable torque under power constraints is calculated as:

$$T_{power} = \frac{P_{max}}{\max(|\omega|, \epsilon)} \tag{3.18}$$

where P_{max} is the maximum motor power, ω is the motor speed, and ϵ is a small positive constant introduced to avoid numerical singularities at low speed.
Although power limits are already considered in the upstream torque allocation process, this additional constraint is retained as a secondary protection layer to ensure that the motor operation remains within safe limits under all conditions.
Second, a temperature-dependent torque limit is introduced to account for thermal protection. The allowable torque is adjusted based on the motor temperature T_m using a piecewise linear strategy:

- At low temperatures, the motor can operate at peak torque.
- As the temperature increases, the allowable torque decreases linearly from peak torque to rated torque.
- At higher temperatures, the allowable torque further decreases from rated torque to zero.
- When the temperature exceeds a critical threshold, the system completely disables torque output to prevent damage.

The system determines the final allowable torque by combining both constraints:

$$T_{max} = \min(T_{power}, T_{thermal}) \tag{3.19}$$

The system then limits the commanded torque within this allowable range:

$$T_{act} = \text{sat}(T_{cmd}, \pm T_{max}) \tag{3.20}$$

This hard protection mechanism ensures that the motor operates within electrical and thermal limits. The mechanism also improves system robustness and prevents unrealistic operating conditions in the simulation.

This study applies the same protection strategy to all three architectures to ensure a fair comparison.

3.5 Motor Loss Evaluation

3.5.1 Motor Loss Evaluation Based on Scaled Efficiency Maps

The motor loss evaluation module calculates the power losses of each electric machine according to its operating point, which is defined by motor torque and rotational speed. In this study, motor losses are evaluated using loss maps, where the instantaneous power loss is obtained through two-dimensional interpolation of pre-defined lookup tables. This approach enables an accurate representation of operating-point-dependent losses and avoids the need for simplified analytical loss models.

For the baseline architecture (Model 1), a measured loss map corresponding to a 200 kW electric machine is available and directly used in the simulation. However, for the other architectures (Model 2 and Model 3), motors with different power ratings (100 kW and 300 kW) are required, for which no experimental loss maps are available.

To address this limitation, a scaling-based approach is adopted to generate the loss maps of motors with different sizes. This method is based on the assumption that motors with similar electromagnetic design exhibit comparable efficiency characteristics when normalized by torque and speed. It should be noted that this scaling approach relies on the assumption that motors with similar electromagnetic design exhibit comparable efficiency characteristics when normalized by torque and speed. While this assumption may not fully capture all design-specific variations (e.g., differences in magnetic loading, cooling design, or loss distribution), it is considered acceptable for system-level comparative analysis. Therefore, the loss map of a reference motor can be scaled to represent motors of different ratings.

Specifically, the torque axis is scaled proportionally to the desired motor capacity, while the loss values are adjusted accordingly to preserve the overall efficiency trends. This approach is consistent with commonly used motor scaling methods in the literature, where efficiency maps of multi-motor systems are derived from a reference motor through torque scaling [20].

As reported in [20], the efficiency map of multiple motors can be derived from a single reference motor by proportionally scaling the torque capability, while preserving similar efficiency distributions across the operating range.

Based on this principle, this study applies scaling factors of 0.5 and 1.5 to generate the loss maps for the 100 kW motor and 300 kW motor, respectively. The simulation then uses the generated loss maps and efficiency maps for loss evaluation.

This method provides a practical and computationally efficient way to estimate motor losses for motors with different power ratings. The method also maintains consistency between the compared architectures.

The following figures present the generated loss maps and efficiency distributions for each motor3.2 – 3.7.

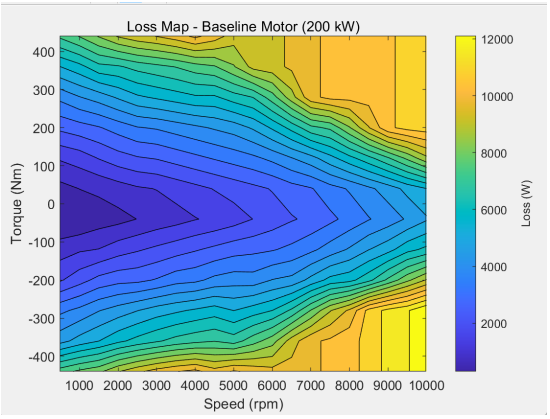

Figure 3.2: Loss Map 200kw

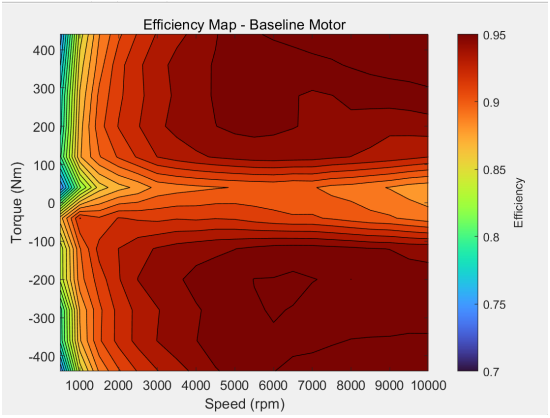

Figure 3.3: Efficiency Map 200kw

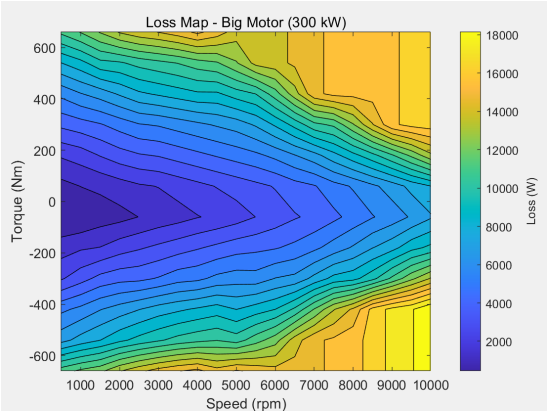

Figure 3.4: Loss Map 300kw

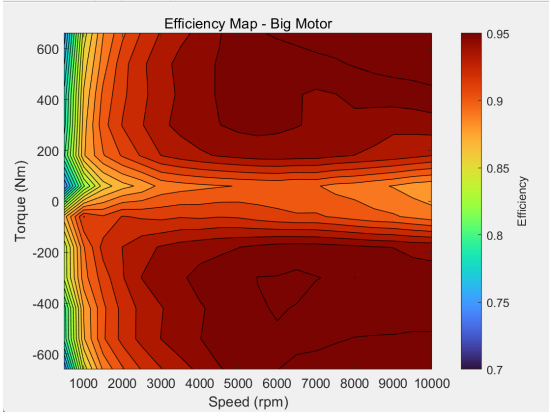

Figure 3.5: Efficiency Map 300kw

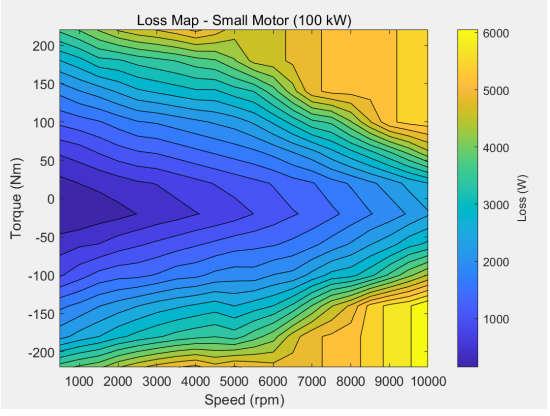

Figure 3.6: Loss Map 100kw

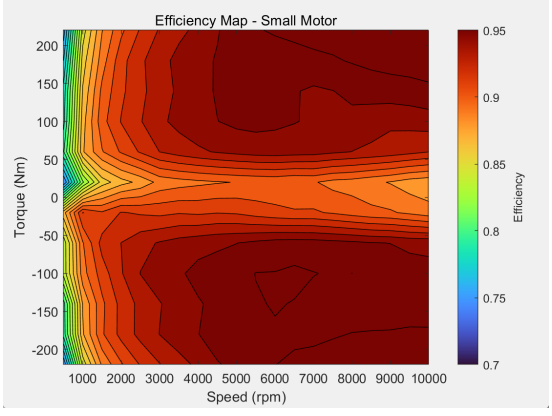

Figure 3.7: Efficiency Map 100kw

Therefore, the scaled efficiency maps are not used to provide exact quantitative predictions of motor losses. Instead, this study uses them to enable a consistent comparison between different drivetrain configurations under the same modeling assumptions.

As all architectures are evaluated using the same scaling methodology, the relative differences in energy consumption are expected to remain meaningful, even if absolute loss values are subject to approximation.

3.5.2 Thermal-Based Loss Modeling Approach

As an alternative to the efficiency map-based method, a physics-based thermal-loss modeling approach was also investigated. This method aims to describe motor losses through analytical loss components and temperature dynamics.

3.5.2.1 Model Formulation

A lumped-parameter thermal model is used to represent the temperature evolution of the electric machine:

$$C\frac{dT_m}{dt} = P_{loss} - P_{cool} \tag{3.21}$$

where C is the thermal capacity and T_m denotes the average motor temperature. The motor losses are modeled as the sum of several components:

$$P_{loss} = P_{cu} + k_h|\omega| + k_{w2}\omega^2 + P_{const} \tag{3.22}$$

The copper loss is temperature-dependent:

$$P_{cu} = k_{cu}\left[1 + \beta(T_m - T_{mref})\right]T^2 \tag{3.23}$$

Cooling is approximated using a linear heat transfer model:

$$P_{cool} = (h_{air} + h_{liq})(T_m - T_{amb}) \tag{3.24}$$

This formulation provides a simplified physical interpretation of motor losses and thermal behavior.

3.5.2.2 Model Calibration and Validation

The study calibrates the thermal-loss model using the available loss data from the baseline motor. The model parameters are adjusted to achieve reasonable temperature levels and loss magnitudes.

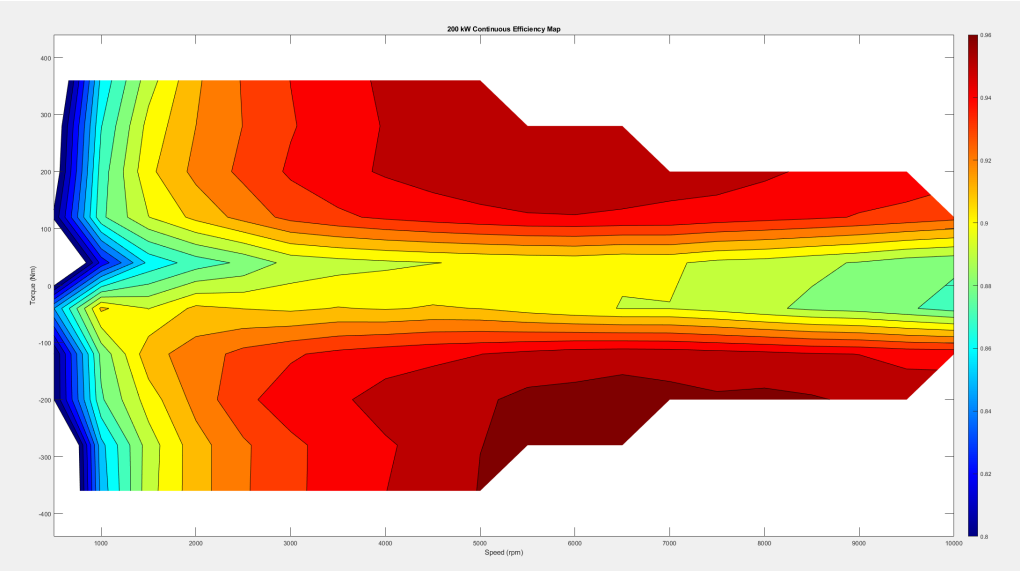

Figure 3.8: Measured efficiency map of the baseline motor

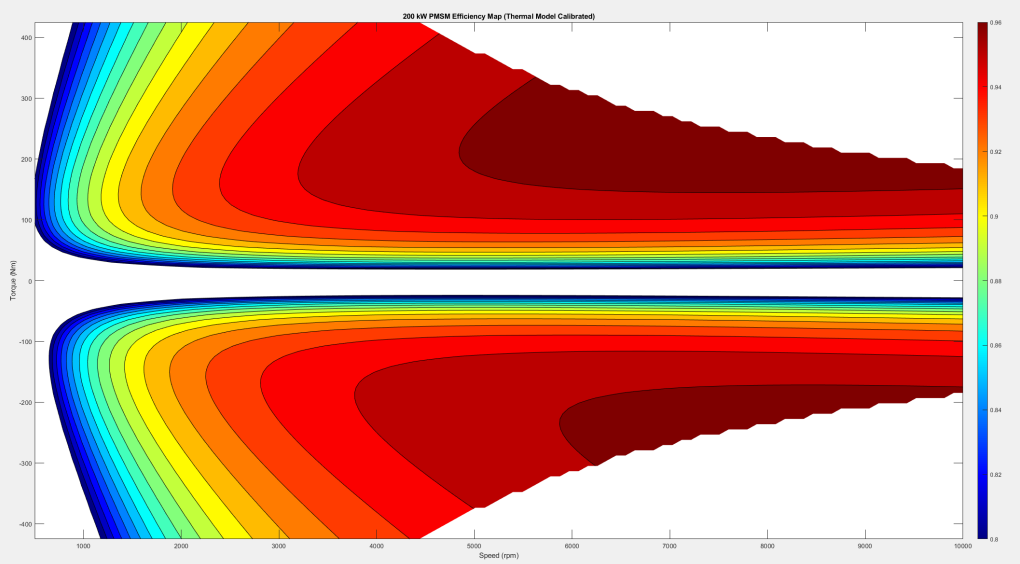

Figure 3.9: Efficiency map reconstructed from the thermal-loss model

To evaluate the model accuracy, this study compares the efficiency map reconstructed from the thermal-loss model with the measured efficiency map. Figure 3.8 shows the measured efficiency map of the baseline motor. Figure 3.9 shows the efficiency map reconstructed from the thermal-loss model.

The comparison shows that the thermal-loss model captures the general efficiency distribution and the main operating regions. However, the model still shows noticeable differences in contour shape and efficiency values across the torque-speed region.

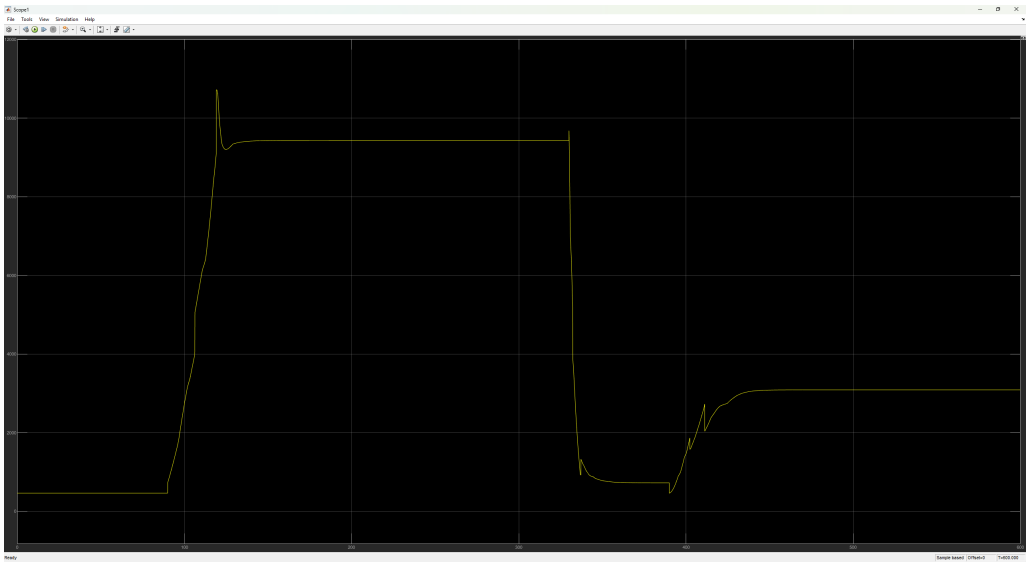

Figure 3.10: Measured motor power loss under a representative operating cycle

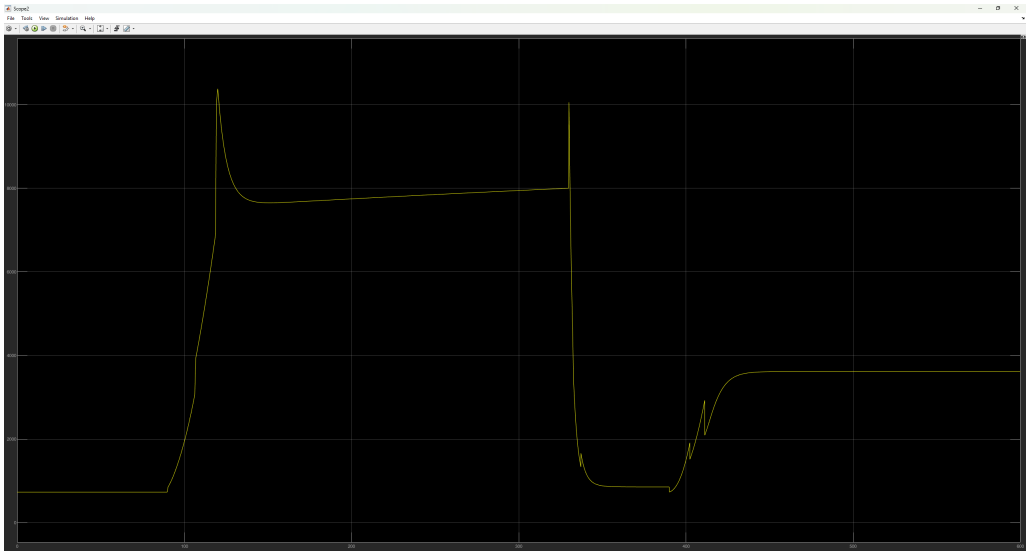

Figure 3.11: Simulated motor power loss from the thermal model

This study also compares simulated power losses with measured losses under the same operating cycle. Figure 3.10 shows the measured motor power loss during a representative operating cycle. Figure 3.11 shows the simulated motor power loss from the thermal-loss model.

The results show that the model captures the overall trend of motor power loss. However, we can still obeserve some differences during transient conditions and in high-loss operating regions. These differences are mainly from the simplified electromagnetic loss model and the limited capability of the analytical model to capture efficiency changes at different operating points.

3.5.3 Comparison of Loss Modeling Approaches

This study compares two motor loss modeling approaches: the efficiency map-based method and the thermal-based analytical method.
The efficiency map-based method uses measured or scaled efficiency data directly. This approach can represent efficiency variations across different torque and speed operating points more accurately. Therefore, it reflects the actual motor performance better under different driving conditions.
The thermal-based analytical model estimates motor losses using simplified equations. Although this method can describe the general loss trend, it cannot fully show detailed efficiency variations, particularly in highly nonlinear operating regions.
The comparison results demonstrate that the efficiency map-based approach provides higher accuracy in both steady-state efficiency representation and dynamic loss prediction. This is particularly important for the present study, where energy consumption differences between architectures are primarily driven by variations in motor operating points.
Therefore, the efficiency map-based method is adopted as the primary loss modeling approach in this study, as it offers better fidelity and is more suitable for architecture-level energy consumption analysis.

3.6 Energy Accumulation Module

The energy accumulation module is used to evaluate the total energy consumption of the vehicle based on motor operating conditions and loss calculations. The module's structure is shown above.

3.6.1 Mechanical Power Calculation

The mechanical power of each motor is calculated based on the motor torque and rotational speed:

$$P_{\text{mech}} = T \cdot \omega \tag{3.25}$$

where T is the motor torque and ω is the motor angular speed.
Since the motor can operate in both driving and regenerative modes, the sign of the mechanical power is used to distinguish between power consumption and power recovery.

3.6.2 Electrical Power Estimation

The system calculates the total electrical power of each motor by combining mechanical power and motor losses:

$$P_{\text{elec}} = \begin{cases} P_{\text{mech}} + P_{\text{loss}}, & P_{\text{mech}} \geq 0 \\ P_{\text{mech}} - P_{\text{loss}}, & P_{\text{mech}} < 0 \end{cases} \tag{3.26}$$

where P_{loss} represents the motor loss obtained from the loss evaluation module.

This formulation ensures the following operating behavior:

- In traction mode, the electrical power includes the useful mechanical output power and the motor losses.
- In regenerative mode, the system subtracts the losses from the recovered mechanical power to represent conversion inefficiency.

Total Power Aggregation

The system calculates the total electrical power demand by summing the electrical power of both motors:

$$P_{\text{total}} = P_{\text{elec},1} + P_{\text{elec},2} \tag{3.27}$$

This total power represents the instantaneous power exchanged with the battery.

Energy Consumption Calculation

The system calculates cumulative energy consumption by integrating the total electrical power over time:

$$E = \int P_{\text{total}}\, dt \tag{3.28}$$

This value represents the net energy drawn from the battery during the operating cycle.

State of Charge Estimation

The system estimates the battery state of charge (SOC) according to the accumulated energy:

$$\frac{d, SOC}{dt} = -\frac{P_{\text{total}}}{E_{\text{bat}}} \tag{3.29}$$

where E_{bat} represents the nominal battery energy capacity.
The model also constrains the SOC within physical limits to ensure numerical stability and realistic system behavior.

Modeling Assumptions

In this study, the battery is modeled as an ideal energy source without internal resistance or dynamic voltage effects. Therefore, the calculated energy consumption directly represents the drivetrain power demand.
This simplification is acceptable because the main objective of this study is to compare the relative energy consumption of different drivetrain architectures under the same operating conditions, rather than to investigate detailed battery dynamics.

3.7 Summary

This chapter presented the unified modeling framework used for the comparative analysis of the investigated dual-motor drivetrain architectures. The developed model combines vehicle longitudinal dynamics, transmission behavior, torque distribution, motor loss evaluation, and energy accumulation within a consistent forward energy flow framework.

Although the three drivetrain architectures differ in coupling characteristics, motor configuration, and transmission layout, the same modeling methodology and operating assumptions are applied to all cases. This ensures that the differences observed in motor operating behavior and energy consumption can be associated primarily with drivetrain configuration and torque distribution characteristics rather than inconsistencies in the simulation framework itself.

Particular attention was given to the representation of motor operating points and operating-point-dependent losses, since the interaction between drivetrain configuration and motor efficiency forms an important part of the energy consumption analysis in this study. For this purpose, the efficiency-map-based loss evaluation method was adopted as the primary approach due to its ability to preserve the operating characteristics of the electric machines under different load conditions.

Overall, the developed modeling framework provides the basis for the comparative evaluation presented in the next chapter, where the energy consumption characteristics of the three drivetrain architectures are investigated under representative articulated hauler operating conditions.

4

Energy Consumption Evaluation under Representative Operating Conditions

Following the drivetrain development and modeling framework introduced in the previous chapters, this chapter presents the comparative simulation results of the investigated dual-motor drivetrain architectures under representative articulated hauler operating conditions. The main objective is to evaluate how different drivetrain configurations affect system operating behavior and energy consumption under realistic heavy-duty driving conditions.

This study selects two representative driving scenarios from real operating data provided by the company. These scenarios represent typical traction-dominated operating conditions for articulated haulers. The selected scenarios include an uphill scenario and a flat-road scenario.

The study evaluates each scenario under both loaded and unloaded conditions. This approach allows the study to investigate how payload variation affects drivetrain performance. The method also provides a consistent comparison of different drivetrain architectures under realistic operating conditions.

Although downhill scenarios are common in articulated hauler operation, this study does not include them. Downhill driving mainly involves regenerative braking and energy recovery. However, this study mainly focuses on torque distribution and its influence on energy consumption during traction-dominated operation.

4.1 Driving Scenarios

Each driving scenario includes time-varying vehicle speed and road gradient profiles. The simulation model uses these profiles as inputs to calculate the required traction demand. The following subsections describe the characteristics of each scenario.

4.1.1 Uphill Scenario

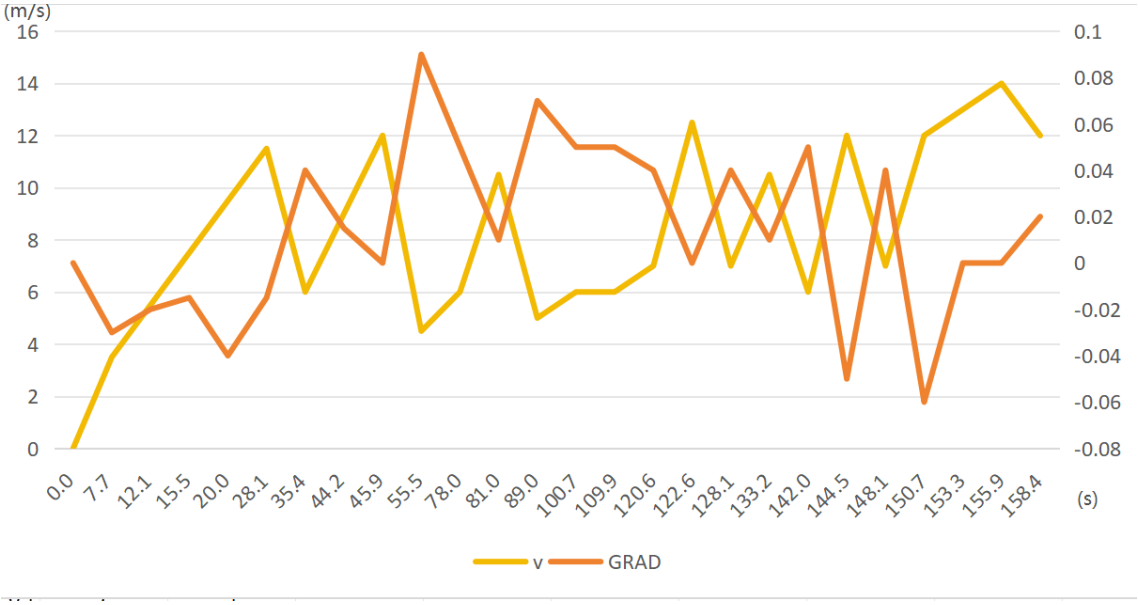

Figure 4.1: Uphill driving scenario

The uphill scenario represents an articulated hauler operating on terrain with noticeable positive road gradients. The figure above shows the vehicle speed profile and road gradient profile.

This study performs simulations under both loaded and unloaded conditions. Under the loaded condition, the vehicle carries a payload of about 55,000 kg. Under the unloaded condition, the payload is much lower.

The speed data shows that the vehicle operates between about 3 m/s and 14 m/s. This test cycle contains repeated acceleration and deceleration phases, indicating that the driving condition is highly dynamic rather than a constant-speed cruising scenario. The continuously varying vehicle speed reflects frequent changes in traction demand throughout the cycle.

In addition, the road gradient changes significantly. The slope profile changes between downhill and uphill sections. And several segments exhibiting relatively steep positive gradients. These uphill conditions substantially increase the traction requirement, particularly when the vehicle is carrying a heavy payload.

The interaction between varying road gradients and payload conditions creates a highly demanding operating environment for the drivetrain. Under such conditions, the drive system must deliver sustained high torque while continuously adapting to changing terrain characteristics. Therefore, this operating scenario provides an appropriate basis for evaluating the influence of drivetrain architecture and torque distribution strategies on overall energy consumption.

4.1.2 Flat-Road Scenario

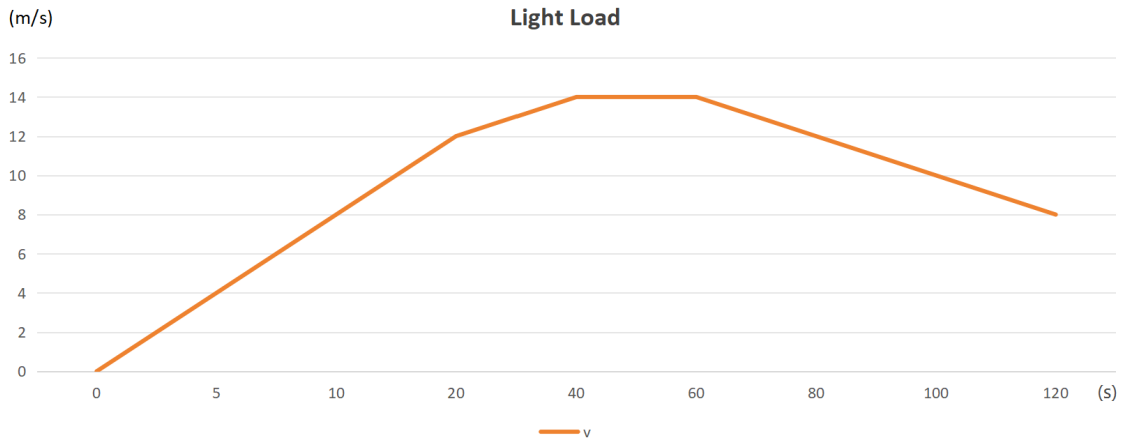

Figure 4.2: Flat-road driving scenario

The flat-road scenario represents an articulated hauler operating on level terrain. The figure above shows the vehicle speed profile and road gradient profile.
Similar to the uphill scenario, this study performs simulations under both loaded and unloaded conditions. This allows the study to evaluate the influence of payload variation under lower traction demand.
The figure shows that the road gradient remains close to 0% during the entire driving cycle, which indicates flat terrain. Under this condition, rolling resistance and vehicle acceleration mainly determine the traction demand.
The vehicle accelerates from standstill to a maximum speed of about 14 m/s. The vehicle then enters a relatively stable high-speed phase before gradually decelerating. Compared with the uphill scenario, the required torque is much lower, especially under unloaded conditions.
Under these operating conditions, the drivetrain mainly works in a relatively low-load region. Most motor operating points are located in low-torque regions of the efficiency map. Because of this, the scenario is suitable for evaluating the performance of different drivetrain architectures when traction demand is limited and the possibility for torque redistribution is smaller.

4.2 Simulation Results

In this study, the vehicle speed is designed to track a predefined reference driving cycle. Due to inherent physical constraints of the powertrain model, including the torque and power limitations of electric motors, the actual vehicle speed cannot perfectly replicate the reference profile under high-load operating conditions. Insufficient traction capability under such circumstances inevitably results in minor speed tracking deviations. For all three powertrain architectures investigated in this work, the speed response characteristics and deviation trends maintain high consistency throughout the entire driving cycle. All configurations are constrained by identical physical boundaries, which ensures an equivalent performance baseline for subsequent analysis. Meanwhile, motor torque outputs in all cases are strictly confined within predefined limits during the simulation, with both torque and power constraints fully satisfied at all operating points. This guarantees the physical feasibility of torque distribution strategies and eliminates the impact of unrealistic operating conditions. Accordingly, a fair and reliable energy consumption comparison can be conducted among the three architectures under equivalent performance constraints.
Therefore, this study interprets the differences in energy consumption among the three configurations as the result of integrated system design choices, rather than the isolated effect of a single factor such as drivetrain structure, motor sizing, or control strategy.

4.2.1 Heavy Load Uphill

Model 1

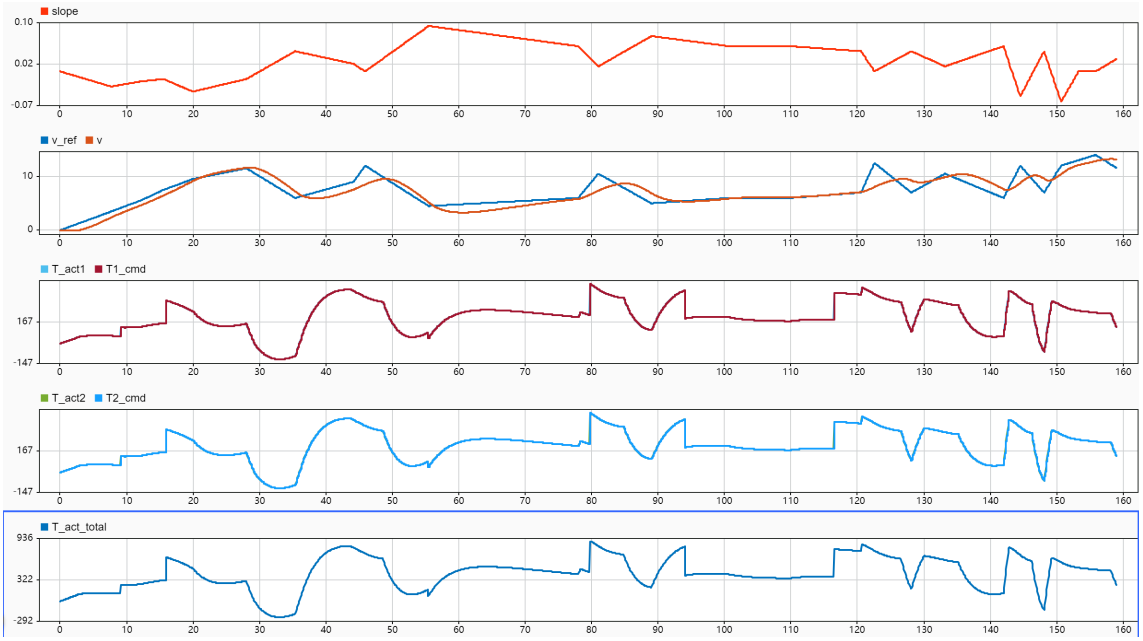

Figure 4.3: Model 1 under Heavy-Load Uphill Condition

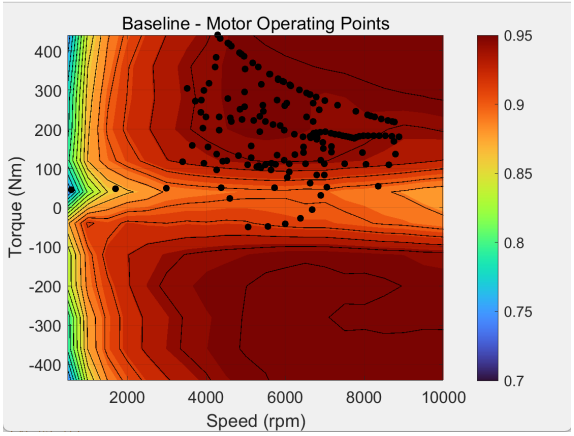

Figure 4.4: Motor Operating Points of Model 1 under Heavy-Load Uphill Condition

Figures 4.3&4.4 show the simulation results and motor operating point distribution of Model 1 under the heavy-load uphill condition.
Model 1 works as the baseline configuration. In this model, the system distributes torque equally between the two motors. Under the heavy-load uphill condition, most operating points are located in the medium-to-high torque region. This distribution reflects the high traction demand during the driving cycle. The total energy consumption of Model 1 is 10.88 kWh, and this value is used as the reference for comparison.

Model 2

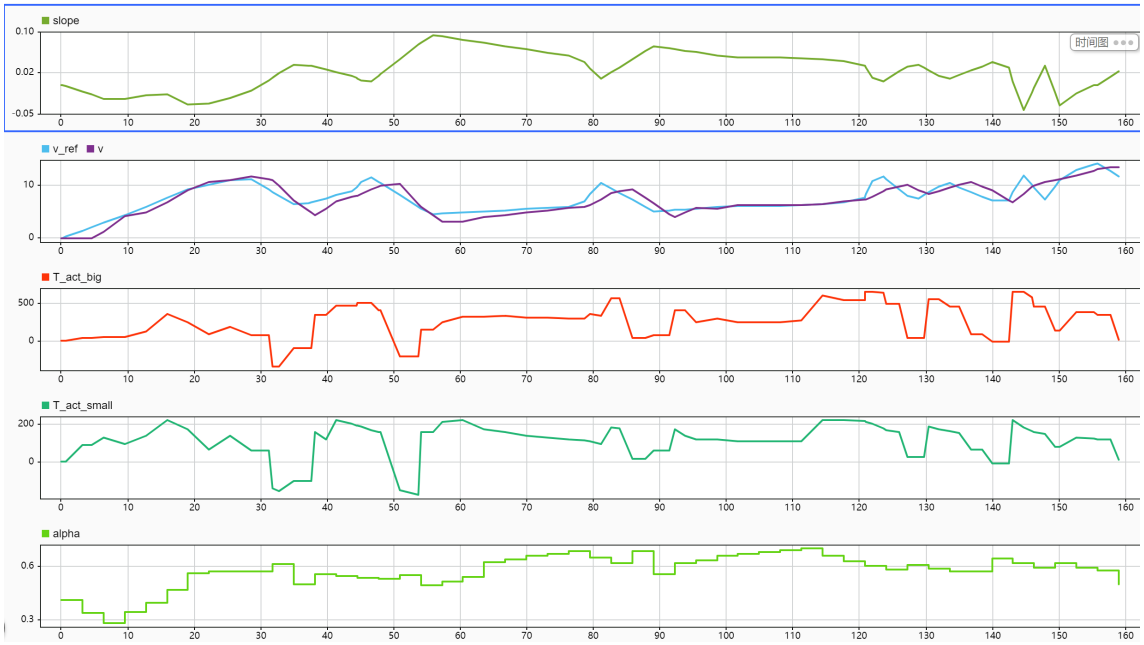

Figure 4.5: Model 2 under Heavy-Load Uphill Condition

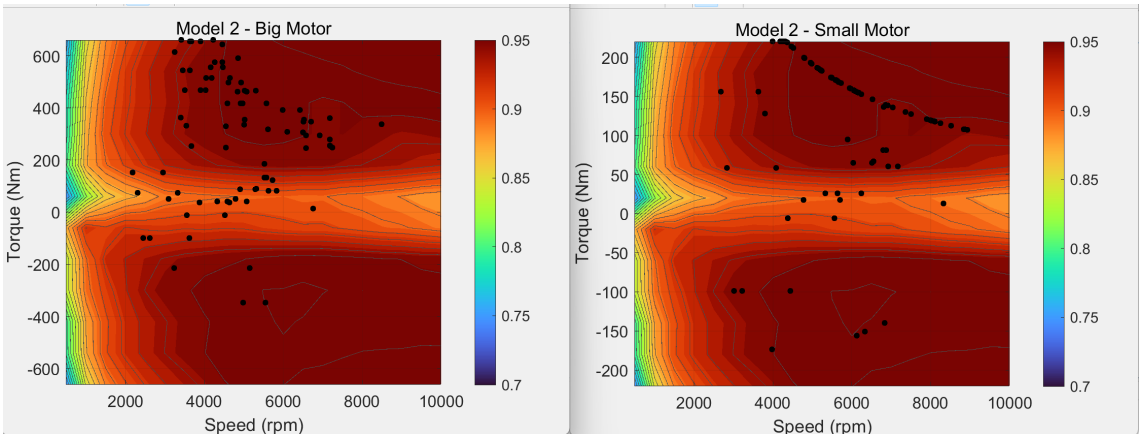

Figure 4.6: Motor Operating Points of Model 2 under Heavy-Load Uphill Condition

Figures 4.5&4.6 show the simulation results of Model 2 under the same operating condition.
Compared with Model 1, Model 2 uses a dynamic torque distribution strategy. Under this operating condition, both motors often operate close to their torque limits because the uphill condition requires high traction demand during most of the driving cycle. The torque allocation generally follows the relative capability of the two motors. The larger motor provides most of the traction torque, while the smaller motor mainly provides additional support when needed.
Figure 4.6 shows the operating point distribution of Model 2. In the positive torque region, which represents traction mode, the operating points do not move significantly toward higher-efficiency regions compared with Model 1. One possible reason is that the motors in Model 1 already operate in medium-to-high torque regions under heavy-load conditions. These operating regions already correspond to relatively high motor efficiency. Because of this, the possibility for additional efficiency improvement in the traction region becomes limited.
Another reason may be that under continuous high-load operation, the torque demand itself dominates the motor operating behavior. Even though Model 2 provides more flexibility in torque allocation, the motors still need to operate in relatively high-torque regions to satisfy the required vehicle traction demand. As a result, the effect of torque redistribution on operating point relocation becomes less noticeable than under lower-load conditions.
In the negative torque region, which represents regenerative operation, Model 2 shows more operating points located in relatively efficient operating areas. This behavior may be related to the different motor speed distributions created by the modified gear ratios. The interaction between torque allocation and changing vehicle operating conditions during the driving cycle may also contribute to this effect. Since regenerative operation depends strongly on motor speed and available regeneration capability, the additional drivetrain flexibility in Model 2 may help some operating points move closer to more efficient regenerative regions.
Although the overall operating point distributions of Model 1 and Model 2 remain generally similar, differences in regenerative operation and overall drivetrain behavior during the driving cycle may still influence the total energy consumption. In

addition, the asymmetric motor configuration and different speed distributions in Model 2 may also contribute to lower overall losses in some operating conditions. The total energy consumption of Model 2 decreases to 9.962 kWh. This corresponds to an energy reduction of about 4.7% compared with Model 1.

Model 3

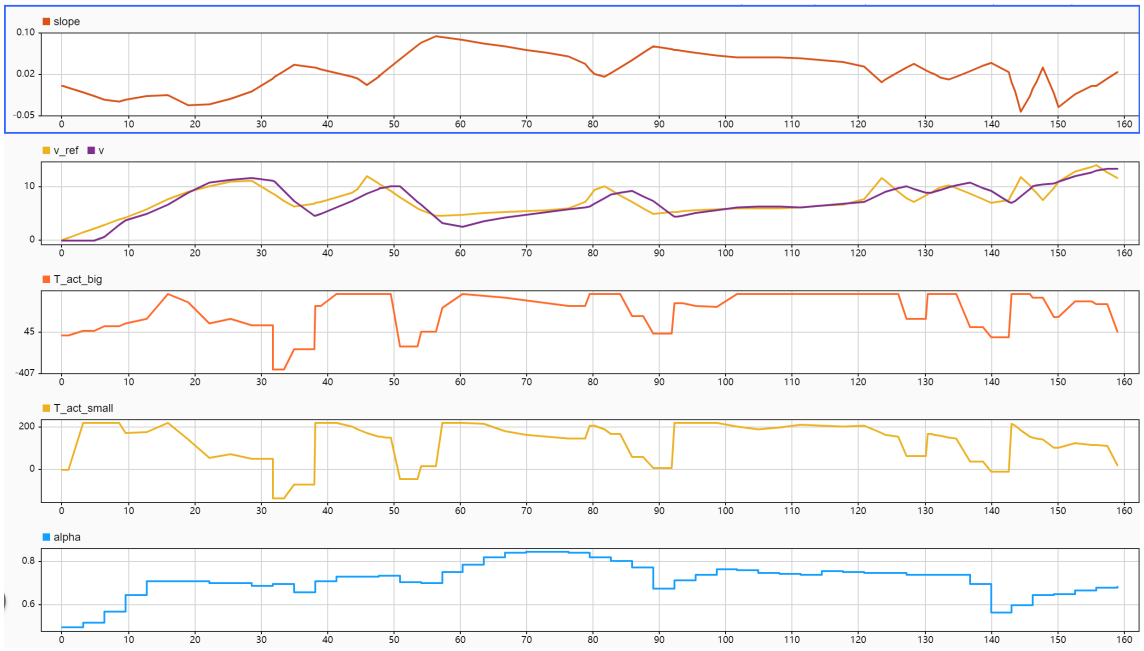

Figure 4.7: Model 3 under Heavy-Load Uphill Condition

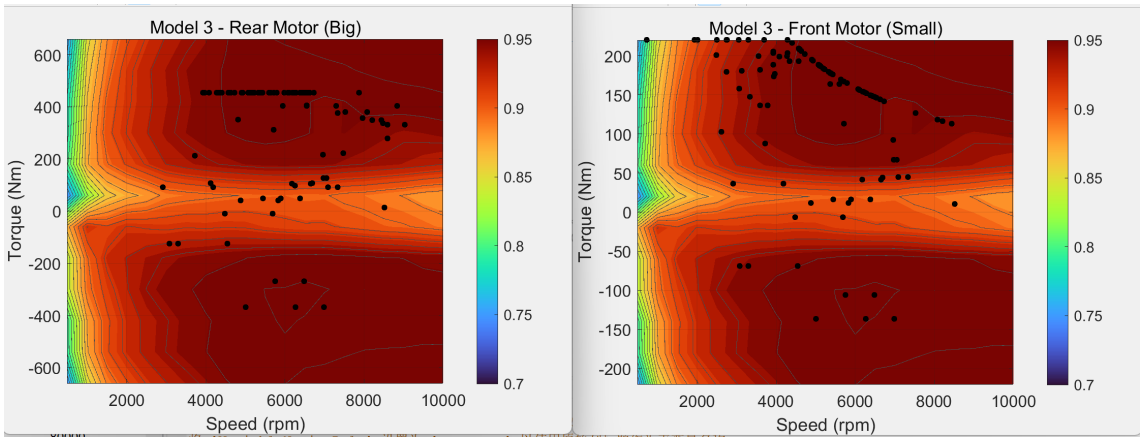

Figure 4.8: Motor Operating Points of Model 3 under Heavy-Load Uphill Condition

Figures 4.7&4.8 show the simulation results of Model 3 under the heavy-load uphill condition.

For Model 3, the operating points appear slightly more dispersed toward lower-efficiency regions compared to the other configurations. Although the overall operating point distribution does not differ drastically, the constrained speed adaptability introduced by the drivetrain configuration may affect the overall motor operating behavior throughout the driving cycle. The resulting total energy consumption increases slightly to 11.01 kWh, corresponding to an increase of approximately 1.2% relative to Model 1.

Overall, under heavy-load uphill conditions, all three architectures mainly operate in medium-to-high torque regions because of the high traction demand. In these regions, the motor efficiencies are already relatively high. Because of this, the differences in operating point distributions in the traction region remain relatively small. This reduces the possibility of achieving large efficiency improvements only through torque redistribution.

Therefore, the differences in energy consumption are likely affected by several factors together. These factors include regenerative operating behavior, drivetrain configuration, motor speed distribution, and power allocation characteristics during the driving cycle. The results indicate that under continuous high-load conditions, torque distribution has a more limited effect on total energy consumption. In contrast, drivetrain configuration and transmission design have a larger influence on system-level efficiency.

4.2.2 Light Load Uphill

Model 1

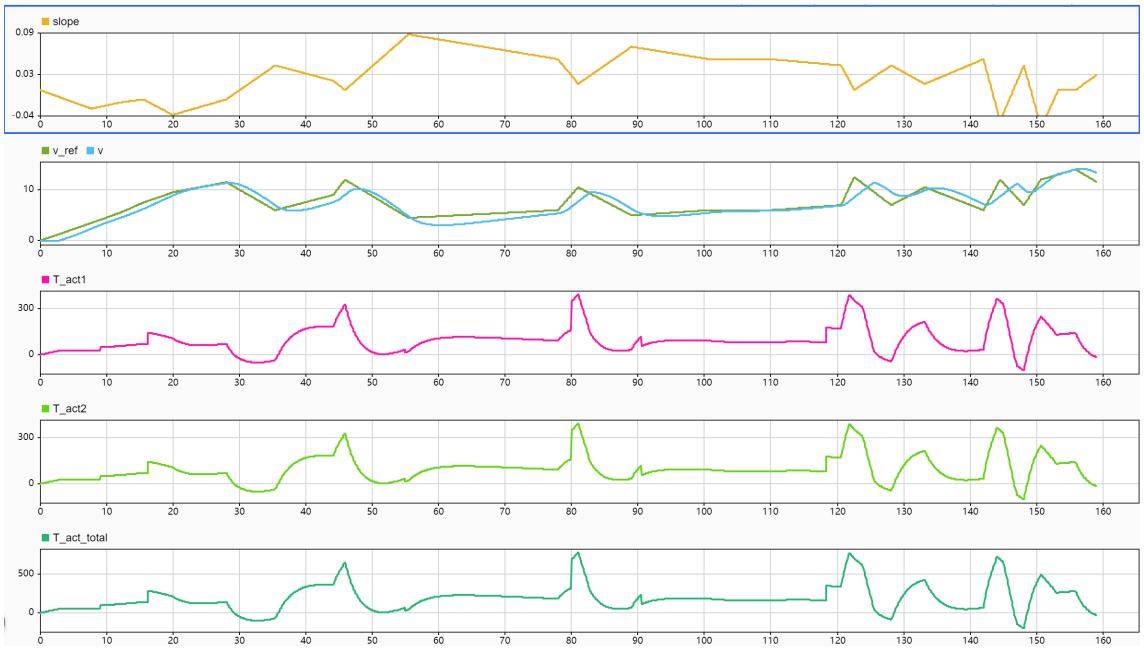

Figure 4.9: Model 1 under Light-Load Uphill Condition

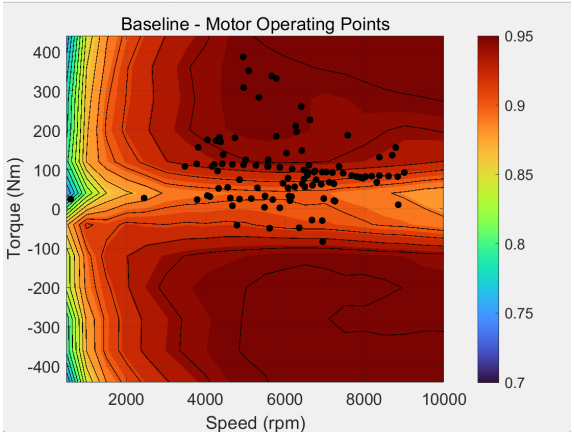

Figure 4.10: Motor Operating Points of Model 1 under Light-Load Uphill Condition

Figures 4.9&4.10 show the simulation results and motor operating point distribution of Model 1 under the light-load uphill condition.
Under the light-load uphill condition, the overall traction demand is lower compared to the previous heavy-load scenario, allowing greater flexibility in torque allocation. Model 1 serves as the baseline configuration, where the torque is evenly distributed between the two motors. Due to the reduced load demand, the operating points are mainly concentrated in the low-to-medium torque region of the efficiency map. The total energy consumption is 5.418 kWh.

Model 2

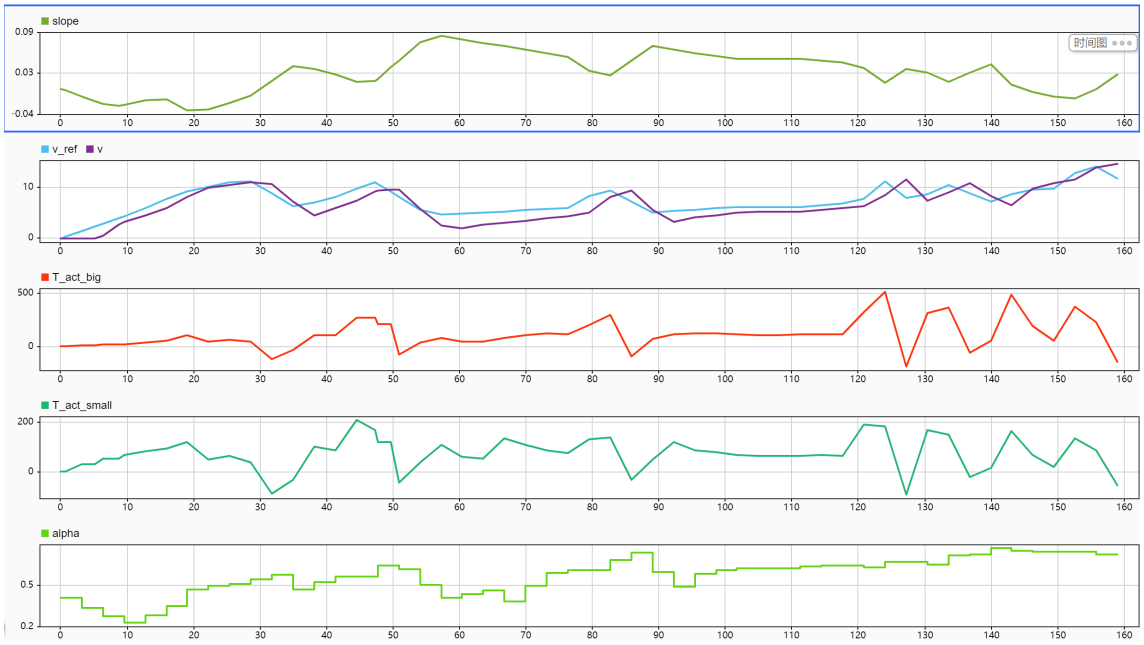

Figure 4.11: Model 2 under Light-Load Uphill Condition

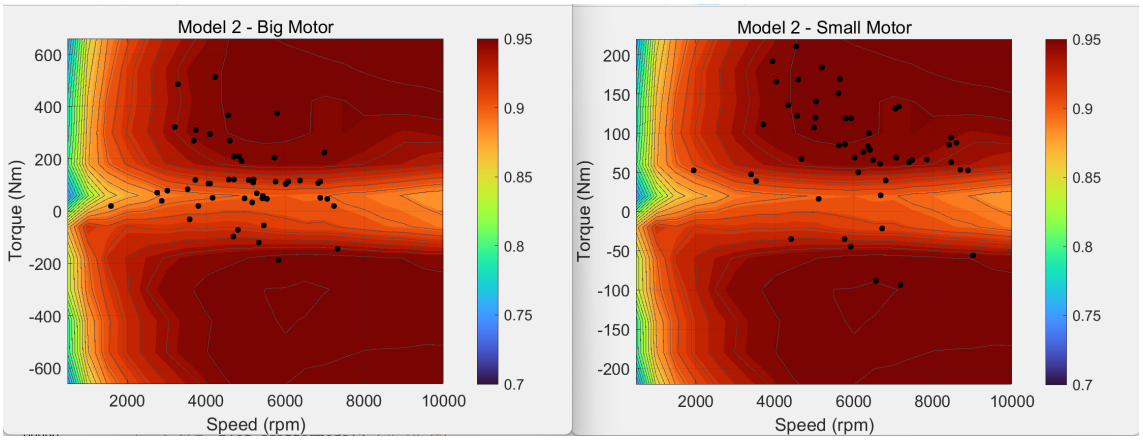

Figure 4.12: Motor Operating Points of Model 2 under Light-Load Uphill Condition

Figures 4.11&4.12 present the corresponding simulation results for Model 2 under the same operating condition.

Compared with Model 1, Model 2 uses a dynamic torque distribution strategy, and this strategy becomes more effective under light-load conditions.

Figure 4.12 shows the operating point distribution of Model 2 under the light-load uphill condition. Compared with Model 1, some operating points move toward relatively higher-efficiency regions. This shift is more noticeable than in the heavy-load uphill condition.

One possible reason is that under lower traction demand, the drivetrain has greater flexibility in torque allocation. The motors no longer need to continuously operate close to their torque limits. Because of this, the controller can distribute torque more freely between the two motors according to their efficiency characteristics. The system can therefore place the motors in more suitable operating regions during different parts of the driving cycle.

The modified drivetrain configuration in Model 2 also contributes to this behavior. Since the two motors operate with different reduction ratios, the motors can work at different rotational speeds. This additional flexibility allows the system to better utilize the efficiency characteristics of each motor, especially under medium and low torque demand.

In addition, the asymmetric motor configuration may improve operating behavior during acceleration, deceleration, and transient load changes. Under light-load conditions, the smaller motor can handle part of the traction demand in relatively efficient operating regions, while the larger motor avoids operating too frequently in lower-efficiency regions. This interaction between drivetrain configuration and torque allocation may help reduce overall system losses during the driving cycle.

Although the changes in operating point distribution are still moderate, the combined effect of torque allocation flexibility, different motor speed distributions, and improved operating behavior contributes to lower total energy consumption.

The total energy consumption of Model 2 decreases to 5.116 kWh. This result corresponds to an energy reduction of approximately 5.6% compared with Model 1.

Model 3

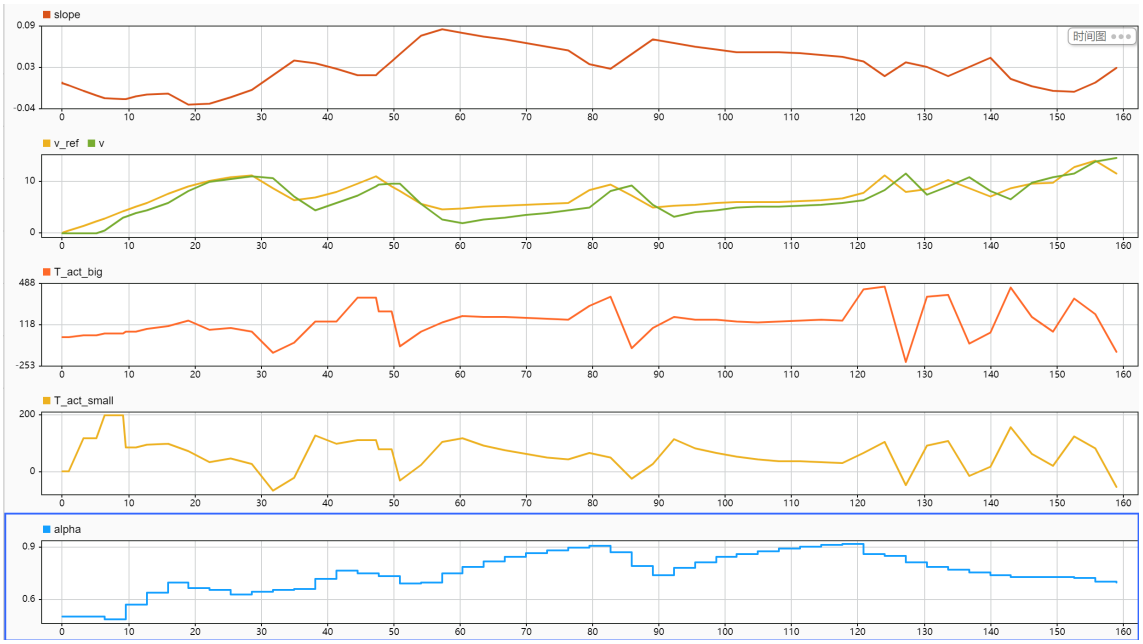

Figure 4.13: Model 3 under Light-Load Uphill Condition

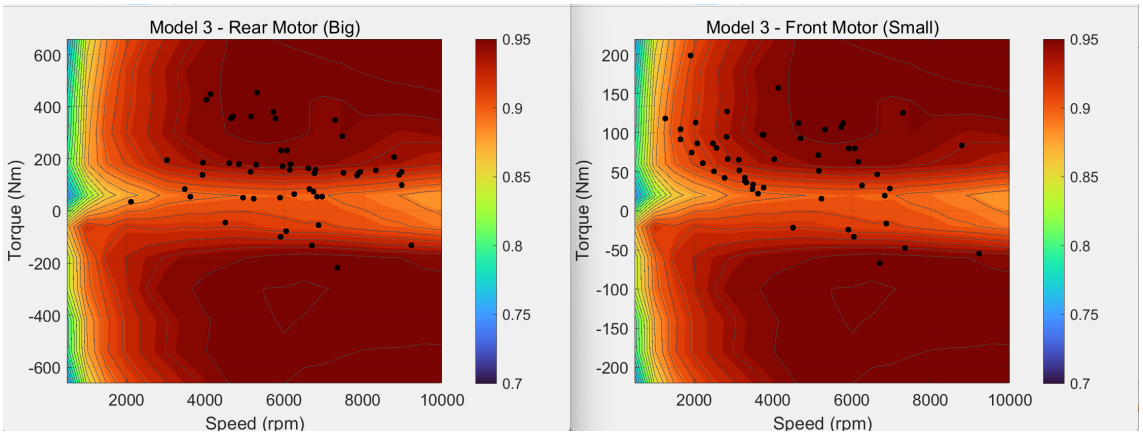

Figure 4.14: Motor Operating Points of Model 3 under Light-Load Uphill Condition

Figures 4.13&4.14 show the simulation results of Model 3 under the light-load uphill condition.
For Model 3, the operating points show a slight tendency to move toward lower-efficiency regions compared with Model 1 and Model 2. This behavior can be observed in both the traction region and some transient operating conditions during the driving cycle.
One possible reason is that the drivetrain configuration of Model 3 limits the speed adaptability of the motors under this operating condition. Although the fully decoupled architecture provides higher structural flexibility, the simplified implementation

used in this study constrains the ability of the motors to fully utilize that flexibility. In particular, the fixed reduction ratio on one axle limits the range of achievable motor operating speeds. As a result, some operating points remain outside the more efficient regions of the motor efficiency map.
Under light-load conditions, the total traction demand is relatively low. Because of this, the influence of motor operating efficiency becomes more sensitive to drivetrain configuration and speed distribution. Small differences in motor operating regions can therefore produce a more noticeable effect on overall energy consumption.
At the same time, the effectiveness of torque redistribution in Model 3 appears limited under this operating condition. Although the architecture allows independent axle control, the operating points do not show a clear shift toward more favorable efficiency regions. This suggests that increased drivetrain flexibility alone does not automatically improve energy efficiency. The benefits also depend on how well the transmission design, gear ratio selection, and torque distribution strategy work together.
The total energy consumption of Model 3 increases to 5.74 kWh. This corresponds to an increase of about 5.9% compared with Model 1.
Overall, under light-load uphill conditions, the lower traction demand provides more flexibility for torque allocation compared with the heavy-load uphill scenario. Because of this, the influence of drivetrain configuration and torque distribution on motor operating behavior becomes more noticeable.
The results indicate that energy consumption under these conditions depends not only on the achievable torque distribution itself, but also on how effectively the drivetrain configuration allows the motors to operate in favorable efficiency regions during the driving cycle.
In this case, Model 2 achieves a moderate reduction in energy consumption because the drivetrain configuration and torque distribution strategy work together more effectively under lower load demand. In contrast, the constrained implementation of Model 3 limits the potential advantage of increased drivetrain flexibility, which reduces the expected efficiency benefit.

4.2.3 Light-load flat-road condition

Model 1

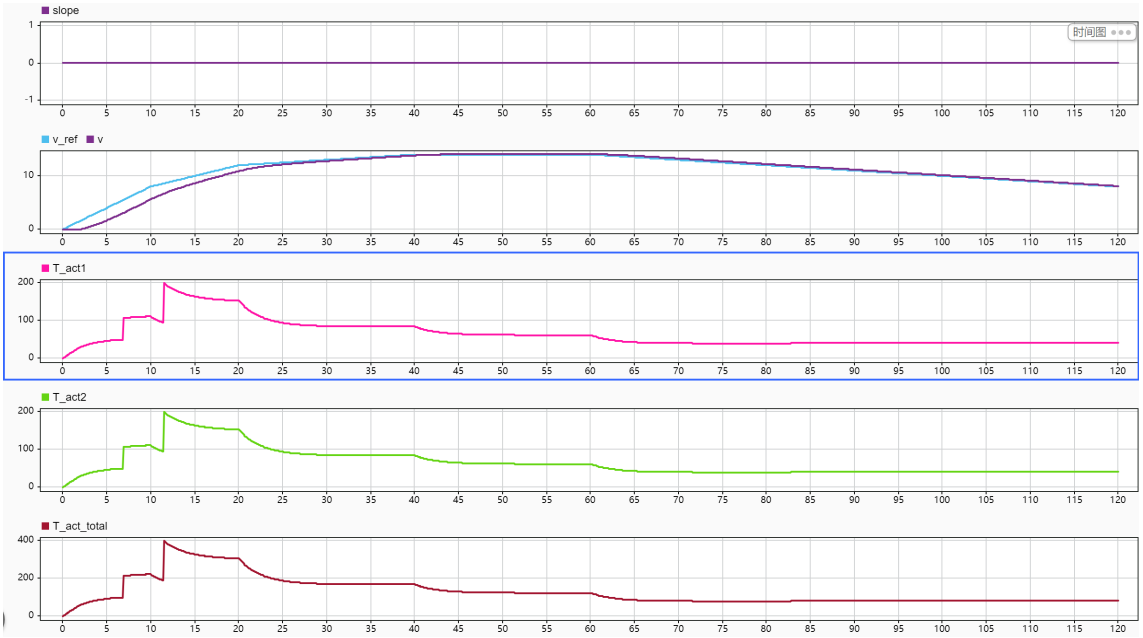

Figure 4.15: Model 1 under Light-Load Flat-Road Condition

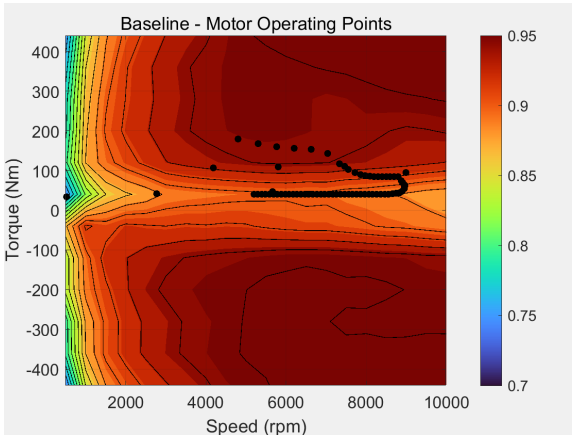

Figure 4.16: Motor Operating Points of Model 1 under Light-Load Flat-Road Condition

Figures 4.15&4.16illustrate the simulation results and operating points distribution of Model 1 under the light-load flat-road condition.
Under the light-load flat-road condition, the traction demand is relatively low and remains stable throughout the driving cycle. As a result, the motors predominantly operate in the low-torque region.
Model 1 serves as the baseline configuration, with an equal torque distribution between the two motors. The operating points are concentrated in a narrow band of low torque and medium-to-high speed. The total energy consumption is 3.542 kWh.

Model 2

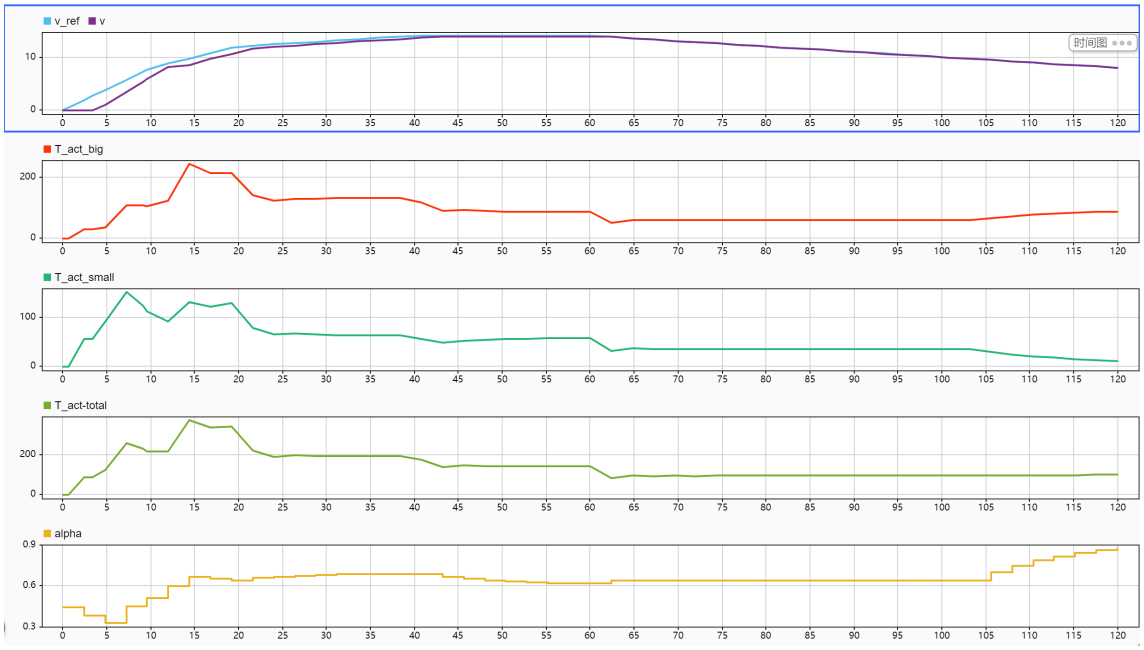

Figure 4.17: Model 2 under Light-Load Flat-Road Condition

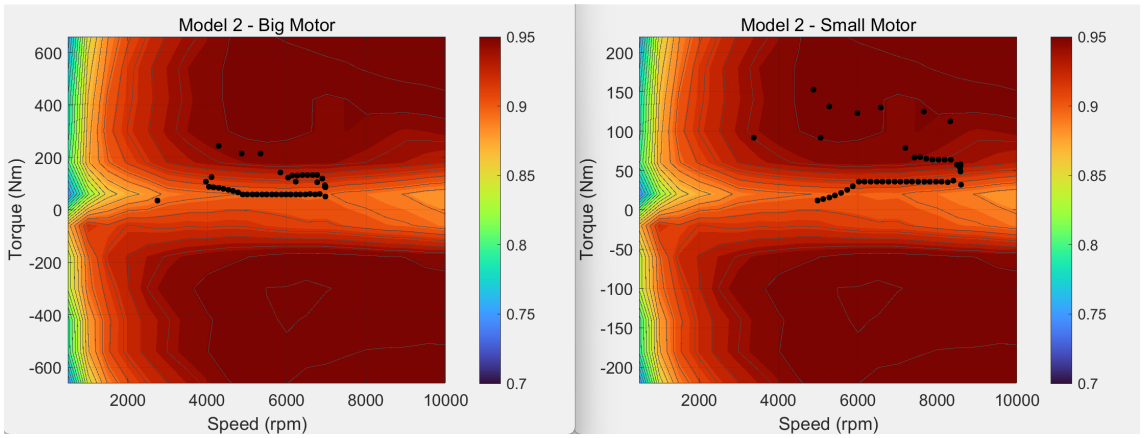

Figure 4.18: Motor Operating Points of Model 2 under Light-Load Flat-Road Condition

Figures 4.17&4.18 present the corresponding simulation results for Model 2 under the same operating condition.
Compared to Model 1, Model 2 continues to employ a dynamic torque distribution strategy under light-load flat-road conditions.
From the operating point distribution shown in Fig. 4.18, a slight shift toward relatively higher-efficiency regions can be observed. Compared to the light-load uphill case, the shift is less pronounced, indicating that the potential for efficiency improvement under this operating condition is more limited.

This behavior is likely related to the relatively low and stable traction demand, which reduces the variation in motor operating conditions throughout the driving cycle. As a result, the flexibility available for torque redistribution becomes more limited compared to uphill scenarios.
Nevertheless, a modest reduction in total energy consumption is still achieved. The total energy consumption decreases to 3.415 kWh, corresponding to a reduction of approximately 3.6% compared to Model 1.

Model 3

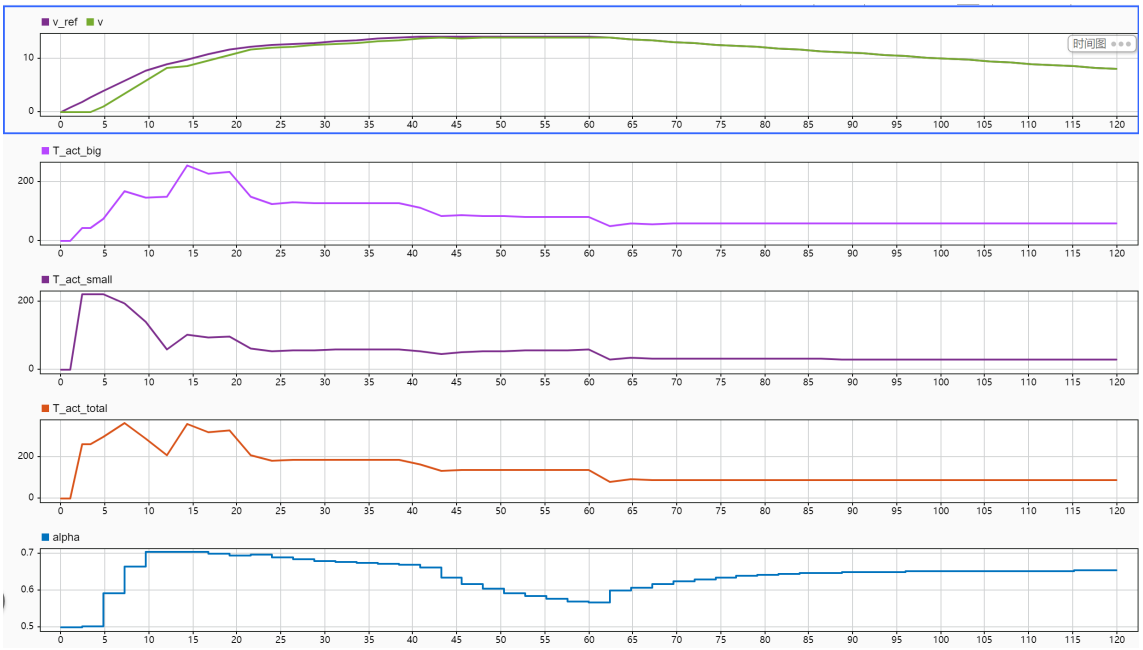

Figure 4.19: Model 3 under Light-Load Flat-Road Condition

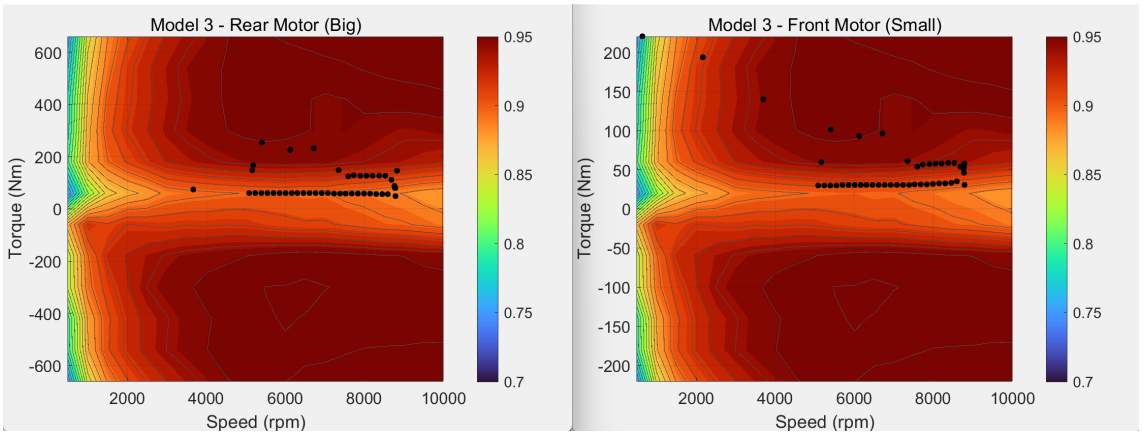

Figure 4.20: Motor Operating Points of Model 3 under Light-Load Flat-Road Condition

Figures 4.19&4.20 show the simulation results of Model 3 under the light-load flat-road condition.

For Model 3, the total energy consumption increases to 3.804 kWh, corresponding to an increase of approximately 7.4% relative to Model 1. The operating points of the motors exhibit a tendency to shift toward lower-efficiency regions compared to the other configurations.

This behavior may be associated with the drivetrain configuration, where the front motor operates with a fixed reduction ratio. As a result, its ability to maintain favorable operating conditions throughout the driving cycle becomes more limited.

Overall, under light-load flat-road conditions, the operating points of all configurations are already concentrated within relatively efficient operating regions due to the low and stable traction demand. Consequently, the available margin for further efficiency improvement through torque redistribution remains relatively limited.

While Model 2 achieves a moderate reduction in energy consumption, the overall differences between the configurations remain relatively small. These results suggest that under steady low-load conditions, the influence of torque distribution strategies becomes less significant, while drivetrain speed adaptability and transmission configuration continue to affect the achievable system efficiency.

4.2.4 Heavy-load flat condition

Model 1

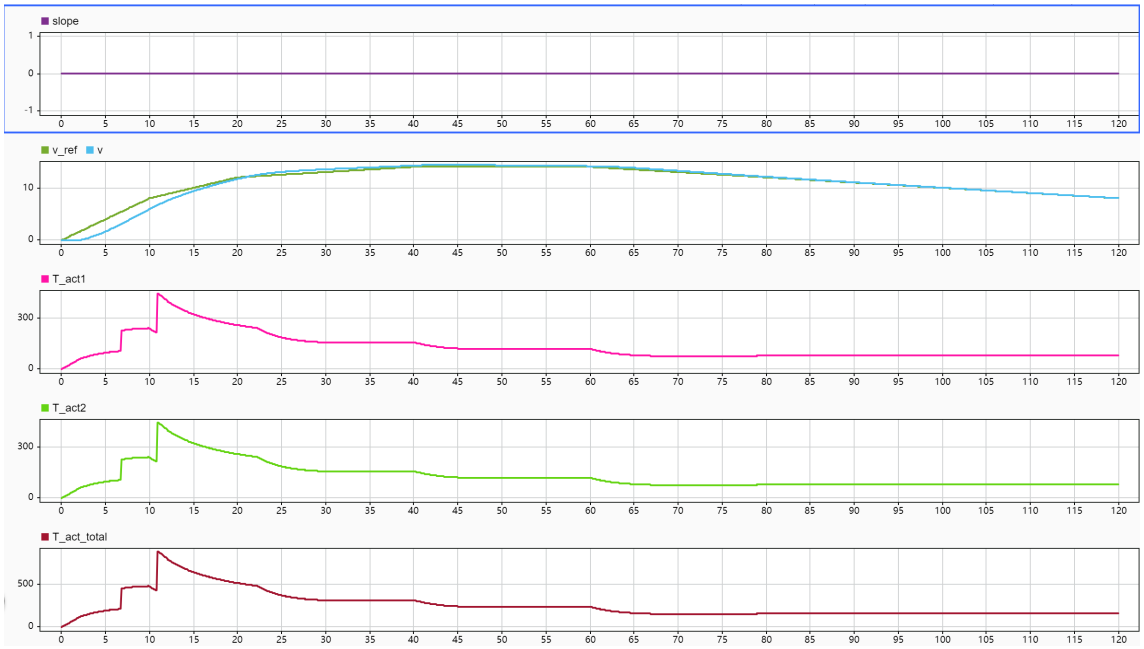

Figure 4.21: Model 1 under Heavy-Load Flat-Road Condition

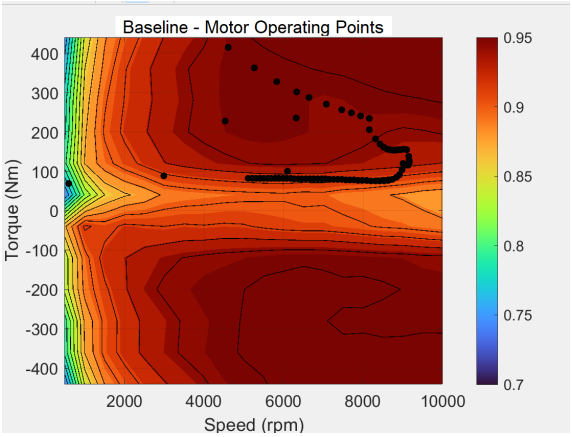

Figure 4.22: Motor Operating Points of Model 1 under Heavy-Load Flat-Road Condition

Figures 4.21&4.22 illustrate the simulation results and operating points distribution of Model 1 under the heavy-load flat-road condition.
Under the heavy-load flat-road condition, the vehicle operates with a high payload while the road gradient remains zero. As a result, the traction demand is primarily determined by the vehicle mass, without additional resistance from road slope. Compared to the light-load flat scenario, the torque demand is increased; however, it remains significantly lower than that observed under heavy-load uphill conditions. Model 1 serves as the baseline configuration, with equal torque distribution between the two motors. The total energy consumption is 6.885 kWh.

Model 2

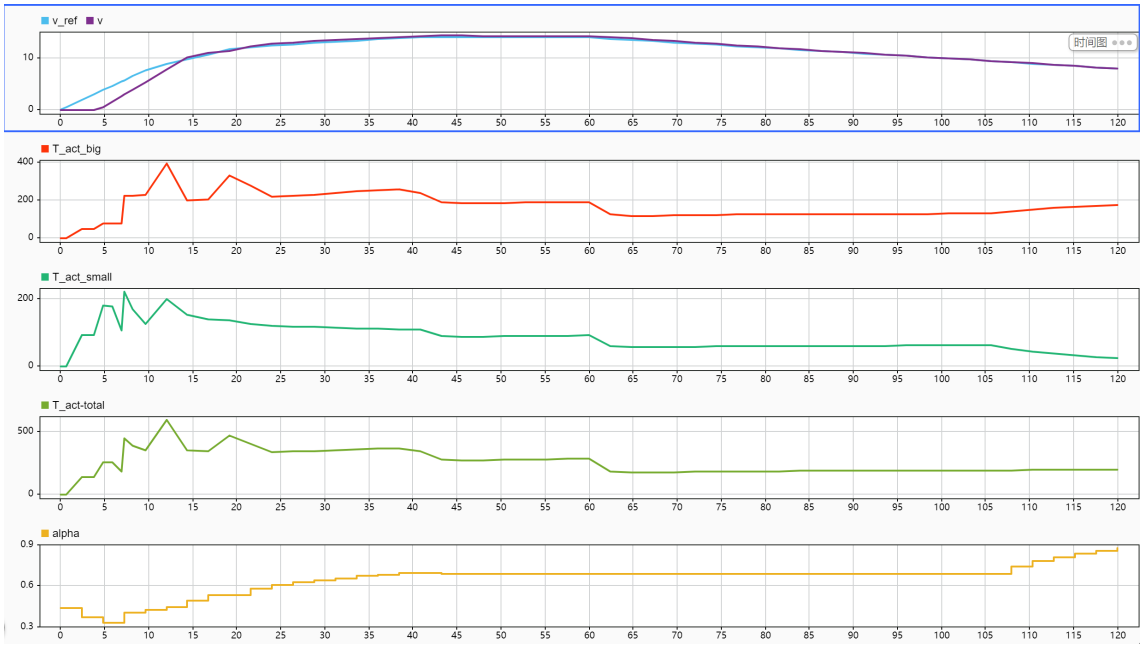

Figure 4.23: Model 2 under Heavy-Load Flat-Road Condition

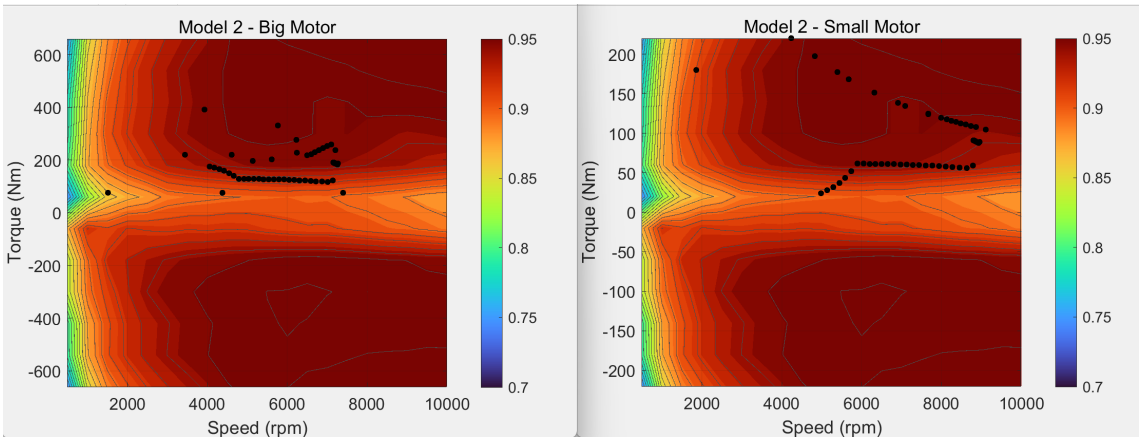

Figure 4.24: Motor Operating Points of Model 2 under Heavy-Load Flat-Road Condition

Figures 4.23&4.24 show the corresponding simulation results for Model 2 under the same operating condition.

Compared with Model 1, Model 2 applies a dynamic torque distribution strategy under the heavy-load flat-road condition. The drivetrain distributes torque between the two motors according to their operating capability and efficiency characteristics during the driving cycle.

Figure 4.24 shows that the motor operating behavior changes compared with the baseline configuration. In particular, the smaller motor operates more frequently in relatively favorable efficiency regions. The larger motor also shows a slightly different operating point distribution compared with Model 1.

Although the overall operating point shift is still moderate, the modified drivetrain configuration and torque allocation strategy continue to influence motor behavior throughout the driving cycle. Under this operating condition, the traction demand remains relatively high, so these operating point differences still affect the total system energy consumption.

In addition, the flat-road condition reduces the influence of large road gradients compared with the uphill scenario. Because of this, the drivetrain has slightly more flexibility in torque allocation and operating point adjustment during some parts of the driving cycle. This may further contribute to improved overall efficiency.

As a result, Model 2 achieves the largest reduction in total energy consumption among all evaluated scenarios. The total energy consumption decreases to 6.113 kWh, which corresponds to an energy reduction of approximately 11.2% compared with Model 1.

Model 3

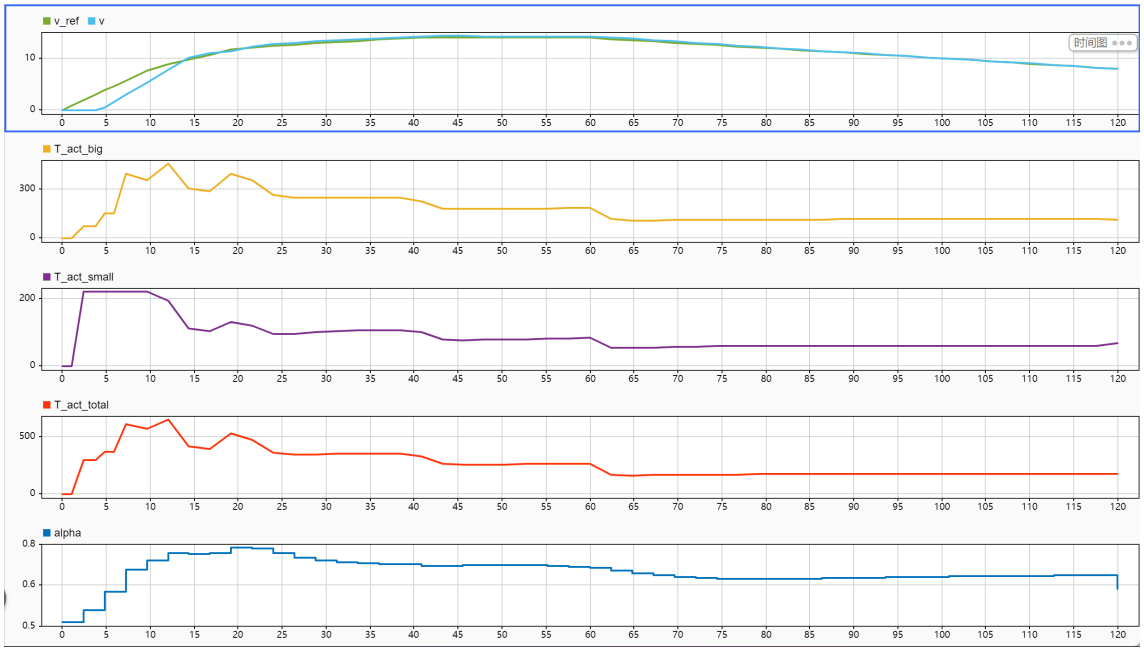

Figure 4.25: Model 3 under Heavy-Load Flat-Road Condition

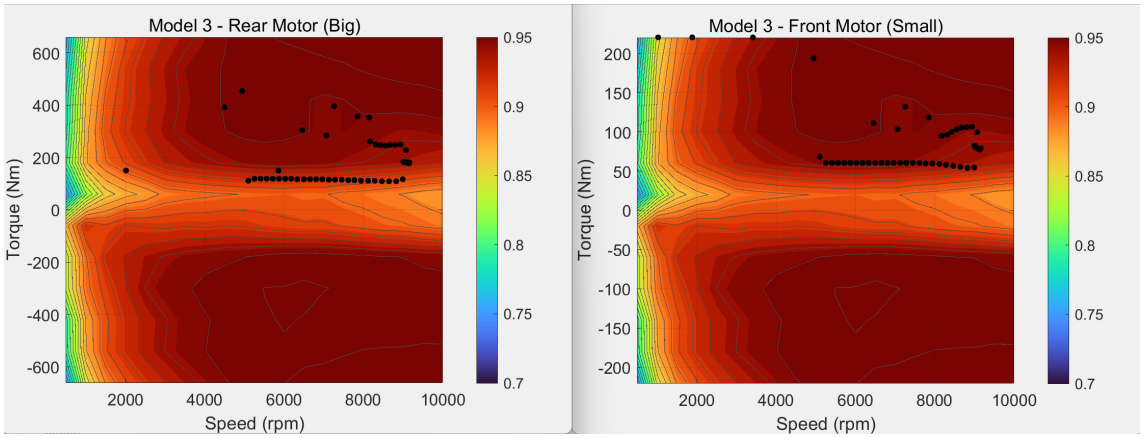

Figure 4.26: Motor Operating Points of Model 3 under Heavy-Load Flat-Road Condition

Figures 4.25&4.26 show the simulation results of Model 3 under the heavy-load flat-road condition.
For Model 3, the total energy consumption increases to 7.243 kWh, representing an increase of approximately 5.2% relative to Model 1. From the operating point distribution, some operating points extend toward relatively lower-efficiency regions compared to Model 1 and Model 2.
This behavior may be related to the drivetrain configuration, where the limited speed adaptability of the front motor affects its ability to maintain favorable operating

conditions throughout the driving cycle. Consequently, the potential benefit of torque redistribution becomes more limited under this configuration.
Overall, under heavy-load flat-road conditions, the motors operate under sustained moderate power demand while avoiding the strong torque limitations observed in the uphill scenario. Although the changes in operating point distribution are not particularly dramatic, the modified drivetrain configuration and torque distribution strategy still lead to differences in motor operating behavior throughout the driving cycle, which may contribute to the larger reduction in total energy consumption observed under this condition.
Taken together with the previous scenarios, these results suggest that the effectiveness of torque distribution depends not only on the load level itself, but also on how the operating condition influences the achievable motor operating behavior over the driving cycle.

4.3 Summary

Table 4.1: Energy Consumption Comparison under Different Operating Conditions

Condition	**Model 1(kWh)**	**Model 2(kWh)**	**Model 3(kWh)**
Heavy-load Uphill	10.88	9.962 (-4.7%)	11.01 (+1.2%)
Light-load Uphill	5.418	5.116 (-5.6%)	5.74 (+5.9%)
Light-load Flat	3.542	3.415 (-3.6%)	3.804 (+7.4%)
Heavy-load Flat	6.885	6.113 (-11.2%)	7.243 (+5.2%)

Based on the analysis of the four representative operating conditions, it can be observed that the effectiveness of torque distribution is influenced by both the load level and the characteristics of the driving condition.
Under high-load conditions, such as the heavy-load uphill scenario, the required torque approaches the operating limits of the motors. In this case, both machines are frequently constrained by their torque and power capabilities, leaving relatively limited flexibility for torque redistribution. Although a reduction in total energy consumption is still observed for Model 2, part of this improvement may also be associated with differences in regenerative operating behavior during downhill segments of the driving cycle. During the uphill traction phase itself, the operating points are already located within relatively efficient regions, limiting the available margin for further optimization.
Under light-load uphill conditions, the torque demand remains sufficiently high to influence efficiency while still allowing greater flexibility in torque allocation. Under this condition, the modified drivetrain configuration and torque distribution strategy are able to influence motor operating behavior more effectively, contributing to a moderate reduction in energy consumption.
Under light-load flat-road conditions, the traction demand is relatively low and stable, and the operating points of all configurations are already concentrated within relatively efficient operating regions. As a result, the available optimization space

becomes more limited, and only modest differences in energy consumption can be observed between the configurations.
For the heavy-load flat-road condition, the load level can be considered moderate-to-low rather than extreme. Compared to the uphill scenario, the motors are less constrained by maximum torque demand while still operating under sustained power demand throughout the driving cycle. Although the shift in operating point distribution is not the most pronounced among all evaluated scenarios, the combination of asymmetric motor sizing, modified gear ratios, and torque distribution strategy may provide more favorable operating conditions for this drivetrain configuration under the heavy-load flat-road scenario. As a result, the largest reduction in total energy consumption is observed under this operating condition.
From the perspective of overall drivetrain design, Model 2 consistently achieves lower energy consumption across all operating conditions investigated in this study. The combination of asymmetric motor sizing, modified gear ratios, and flexible torque distribution provides additional freedom in motor operating behavior, allowing the drivetrain to utilize the available efficiency improvement potential under different operating scenarios.
In contrast, Model 3 highlights some practical limitations associated with the simplified implementation of a fully decoupled architecture considered in this work. Although increased drivetrain flexibility is introduced through independent axle actuation, the fixed reduction ratio of the front motor limits its speed adaptability under certain operating conditions. As a result, the potential benefits of torque redistribution are not fully realized within the current configuration, and the overall energy consumption remains higher than that of Model 1 in all evaluated scenarios.
Overall, the results suggest that the effectiveness of torque distribution depends not only on the load level itself, but also on the extent to which the drivetrain configuration allows meaningful adjustment of motor operating conditions throughout the driving cycle.

5
Conclusion

5.1 Outcome

The results of this study suggest that drivetrain configuration can influence the energy consumption characteristics of dual-motor electric drive systems under heavy-duty operating conditions. Among the evaluated configurations, the partially coupled drivetrain consistently achieved lower energy consumption across all investigated driving scenarios.
The results indicate that the combination of asymmetric motor sizing, modified gear ratios, and torque distribution strategy can provide more favorable operating conditions for the motors under certain operating conditions. The observed improvements were most noticeable under moderate load scenarios, where sufficient power demand existed while the motors were not strongly constrained by their operating limits.
Under extremely high-load conditions, the potential for further efficiency improvement became more limited, as the motors already operated close to their torque capability and within relatively efficient operating regions. Under very low-load conditions, the reduced torque demand similarly limited the achievable benefit of operating point adjustment.
For the fully decoupled configuration investigated in this study, the higher structural flexibility did not result in lower energy consumption. One possible reason is the simplified implementation used in this work. In particular, the front motor uses a fixed reduction ratio, which limits its speed adaptability under some operating conditions.
Overall, the results show that energy efficiency improvement does not depend only on drivetrain architecture. The results are also affected by the combined influence of motor sizing, transmission design, and torque distribution strategy. Therefore, moderate system-level modifications to existing drivetrain configurations may still provide meaningful potential for improving the energy efficiency of heavy-duty electric vehicles.

5.2 Limitations

Several limitations of this study should be acknowledged.
First, the motor loss evaluation is based on scaled efficiency maps derived from the baseline motor. Due to the limited availability of detailed motor data, the efficiency characteristics of alternative motor configurations were approximated using scaling methods and simplified assumptions. As a result, the presented results should be

interpreted primarily as a comparative system-level analysis rather than an exact quantitative prediction of absolute energy consumption.
Second, the fully decoupled configuration investigated in this work adopts a simplified drivetrain implementation. In particular, the front motor operates with a fixed reduction ratio, which limits its speed adaptability under certain operating conditions. Therefore, the observed performance of this configuration should not be interpreted as representing the full potential of fully decoupled multi-motor drivetrains.
In addition, the investigated drivetrain configurations were not globally optimized. The selected motor sizing, gear ratios, and torque distribution strategies were designed to provide representative and practically relevant configurations for comparative evaluation, rather than achieving the theoretical optimum performance of each architecture.
The study is also limited to simulation-based analysis under four representative operating conditions. Although these scenarios were selected to reflect typical heavy-duty articulated hauler operation, real-world vehicle operation may involve more complex and highly transient driving behaviors that are not fully captured in this work.
Finally, this thesis does not include experimental validation. Although the modeling assumptions are based on realistic engineering considerations, future validation using experimental measurements or higher-fidelity vehicle models would improve the reliability of the results and conclusions.

5.3 Future Work

Several possible directions for future work can be identified based on the results and limitations of this study.
First, future studies should include experimental validation to further verify the simulation results presented in this work. Future research may use hardware-in-the-loop testing, prototype vehicle measurements, or experimental drivetrain testing to improve the reliability of the developed models and related conclusions.
Second, more detailed component models could be incorporated in future investigations. In particular, the use of experimentally measured efficiency maps for different motor configurations, together with thermal effects and inverter losses, would improve the fidelity of the drivetrain loss evaluation and provide more accurate quantitative predictions.
Third, the torque distribution strategy adopted in this work was primarily intended for systematic comparative analysis of different drivetrain configurations. Although the implemented strategy provides a useful reference for evaluating the achievable efficiency potential of the investigated architectures, its computational characteristics and response behavior may not be directly suitable for real-time vehicle applications. Therefore, future work could investigate more advanced torque allocation approaches with improved real-time capability, such as predictive or optimization-based control strategies designed for practical onboard implementation.
In addition, the drivetrain configurations investigated in this study were not globally optimized. Future work could perform a combined optimization of motor sizing,

gear ratio selection, and torque distribution strategy in order to further explore the achievable efficiency potential of different drivetrain configurations.
Finally, the present study considered four representative operating conditions for articulated haulers. Future investigations could extend the analysis to more complex and realistic driving cycles, including highly transient operation, mixed terrain conditions, and real-world haulage duty cycles.

Bibliography

[1] R. D. Valentine, J. G. Trasky and D. R. Rippin, "Load Sharing of Dual Motor Grinding Mill Drives," *IEEE Transactions on Industry Applications*, vol. IA-13, no. 2, pp. 161–168, Mar. 1977, doi: 10.1109/TIA.1977.4503382.

[2] A. L. Scott and R. D. Valentine, "Large Grinding Mill Drives Update," *IEEE Transactions on Industry Applications*, vol. IA-18, no. 6, pp. 736–744, Nov. 1982, doi: 10.1109/TIA.1982.4504132.

[3] J. R. Rodriguez *et al.*, "Technical evaluation and practical experience of high-power grinding mill drives in mining applications," *IEEE Transactions on Industry Applications*, vol. 41, no. 3, pp. 866–874, May–June 2005, doi: 10.1109/TIA.2005.847321.

[4] A. H. Hoffmann and J. G. Trasky, "Evaluation of Large Grinding Mill Drives for the Cement Industry," *IEEE Transactions on Industry Applications*, vol. IA-8, no. 1, pp. 59–72, Jan. 1972, doi: 10.1109/TIA.1972.349738.

[5] J. E. Nelson, "Control of Synchronous Motors on a Common Drive," U.S. Patent 3,369,636, Feb. 20, 1968.

[6] A. Bouscayrol *et al.*, "Multi-machine multi-converter system for drives: analysis of coupling by a global modeling," *Conference Record of the 2000 IEEE Industry Applications Conference*, Rome, Italy, 2000, pp. 1474–1481, doi: 10.1109/IAS.2000.882078.

[7] A. Emadi, K. Rajashekara, S. S. Williamson and S. M. Lukic, "Topological overview of hybrid electric and fuel cell vehicular power system architectures and configurations," *IEEE Transactions on Vehicular Technology*, vol. 54, no. 3, pp. 763–770, May 2005, doi: 10.1109/TVT.2005.847445.

[8] Z. Wang, J. Zhou and G. Rizzoni, "A review of architectures and control strategies of dual-motor coupling powertrain systems for battery electric vehicles," *Renewable and Sustainable Energy Reviews*, vol. 162, p. 112455, 2022, doi: 10.1016/j.rser.2022.112455.

[9] A. Boglietti, A. Cavagnino, D. Staton, M. Shanel, M. Mueller and C. Mejuto, "Evolution and Modern Approaches for Thermal Analysis of Electrical Machines," *IEEE Transactions on Industrial Electronics*, vol. 56, no. 3, pp. 871–882, Mar. 2009, doi: 10.1109/TIE.2008.2011622.

[10] J. Torinsson, *Optimizing torque distribution for enhanced energy efficiency in battery electric vehicles*, Doctoral Thesis, 2025.

[11] E. F. Camacho and C. Bordons, *Model Predictive Control*, 2nd ed., Springer, London, 2007.

[12] G. Bertotti, "General properties of power losses in soft ferromagnetic materials," *IEEE Transactions on Magnetics*, vol. 24, no. 1, pp. 621–630, Jan. 1988, doi: 10.1109/20.43994.

[13] D. A. Staton and A. Cavagnino, "Convection Heat Transfer and Flow Calculations Suitable for Electric Machines Thermal Models," *IEEE Transactions on Industrial Electronics*, vol. 55, no. 10, pp. 3509–3516, Oct. 2008, doi: 10.1109/TIE.2008.922604.

[14] P. H. Mellor, D. Roberts and D. R. Turner, "Lumped parameter thermal model for electrical machines of TEFC design," *IEE Proceedings B (Electric Power Applications)*, vol. 138, no. 5, pp. 205–218, Sept. 1991, doi: 10.1049/ip-b.1991.0025.

[15] C. Onwuka and O. Obe, "Analysis of Load Sharing Capability of a Series-Connected Twin Synchronous Motor Drive," *IEEE Access*, vol. 7, 2019.

[16] C. Xu, X. Guo and Q. Xun, "Loss Minimization Based Energy Management for a Dual Motor Electric Vehicle," *2022 IEEE Transportation Electrification Conference and Expo, Asia-Pacific (ITEC Asia-Pacific)*, Haining, China, 2022, pp. 1–6, doi: 10.1109/ITECAsia-Pacific56316.2022.9941890.

[17] Q. Li, Z. Li, J. Tang, Y. Wang, B. Zhang and D. He, "Multi-objective Torque Distribution Strategy for Distributed Drive Electric Vehicles," *Automotive Engineering*, vol. 47, no. 3, pp. 489–498, 2025.

[18] J. Chen, C. Lin, S. Liang and F. Cao, "A MPC-Based Torque Distribution Strategy for Distributed Drive Electric Vehicles," *Proc. 2018 Joint Int. Conf. Energy, Ecology and Environ. and Int. Conf. Electric and Intelligent Vehicles (ICEEE/ICEIV)*, Melbourne, Australia, 2018, pp. 489–498.

[19] M. Ghazali, M. Vukotić, D. Miljavec and A. E. Hartavi, "Temperature-adaptive torque allocation for all wheel drive electric trucks," *Applied Thermal Engineering*, vol. 276, p. 126846, 2025, doi: 10.1016/j.applthermaleng.2025.126846.

[20] K. Kwon, M. Seo and S. Min, "Efficient multi-objective optimization of gear ratios and motor torque distribution for electric vehicles with two-motor and two-speed powertrain system," *Applied Energy*, vol. 259, p. 114190, 2020, doi: 10.1016/j.apenergy.2019.114190.

[21] A. Pennycott, B. De Novellis, A. Sorniotti and P. Gruber, "Reducing the motor power losses of a four-wheel drive, fully electric vehicle via wheel torque allocation," *Proceedings of the Institution of Mechanical Engineers, Part D: Journal of Automobile Engineering*, vol. 228, no. 7, pp. 830–839, 2014, doi: 10.1177/0954407013516106.

[22] Y. Chen and J. Wang, "Adaptive energy-efficient control allocation for over-actuated electric ground vehicles," *IEEE Transactions on Control Systems Technology*, vol. 22, no. 4, pp. 1362–1373, 2014, doi: 10.1109/TCST.2013.2287560.

[23] A. M. Dizqah, B. Lenzo, A. Sorniotti and P. Gruber, "A fast and parametric torque distribution strategy for four-wheel-drive energy-efficient electric vehicles," *IEEE Transactions on Industrial Electronics*, vol. 63, no. 7, pp. 4367–4376, 2016, doi: 10.1109/TIE.2016.2540584.

[24] Volvo Construction Equipment, "Volvo A30 Electric Articulated Hauler." [Online]. Available: https://www.volvoce.com/europe/en/products/electric-machines/a30-electric/ [Accessed: May 6, 2026].

A

Appendix 1

This appendix presents the detailed Simulink implementation diagrams corresponding to the simulation models described in Chapter 3. While the drivetrain architectures and subsystem models are introduced in the main text through analytical descriptions and mathematical formulations, the figures provided here illustrate their corresponding Simulink realizations.

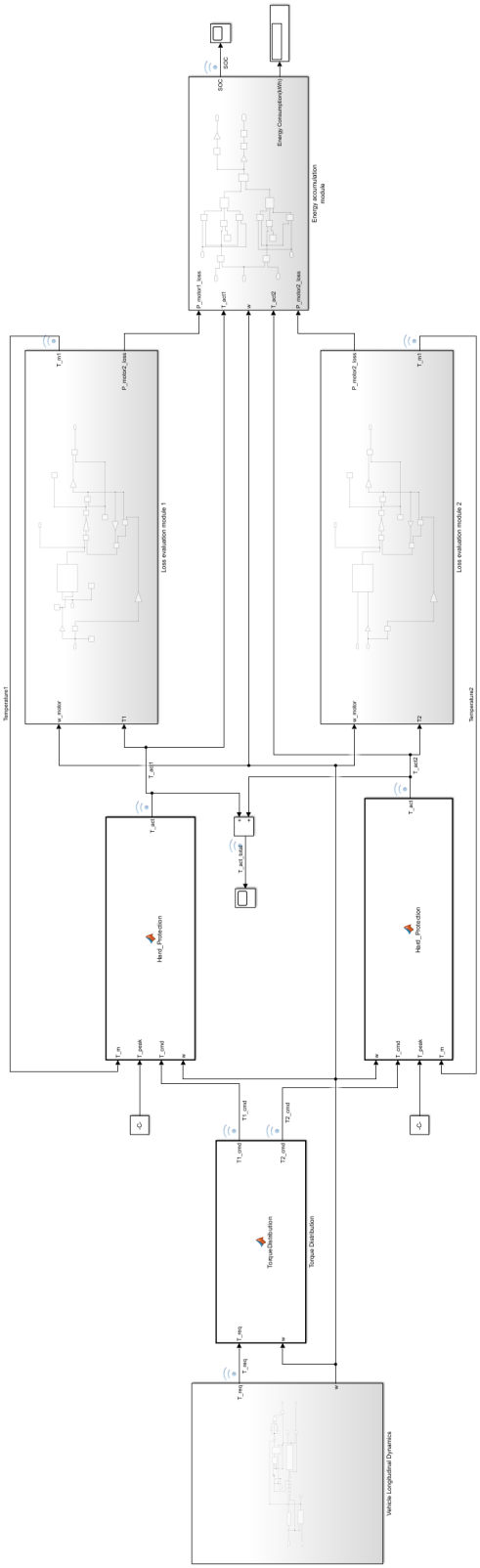

Figure A.1: Overall Modeling Framework

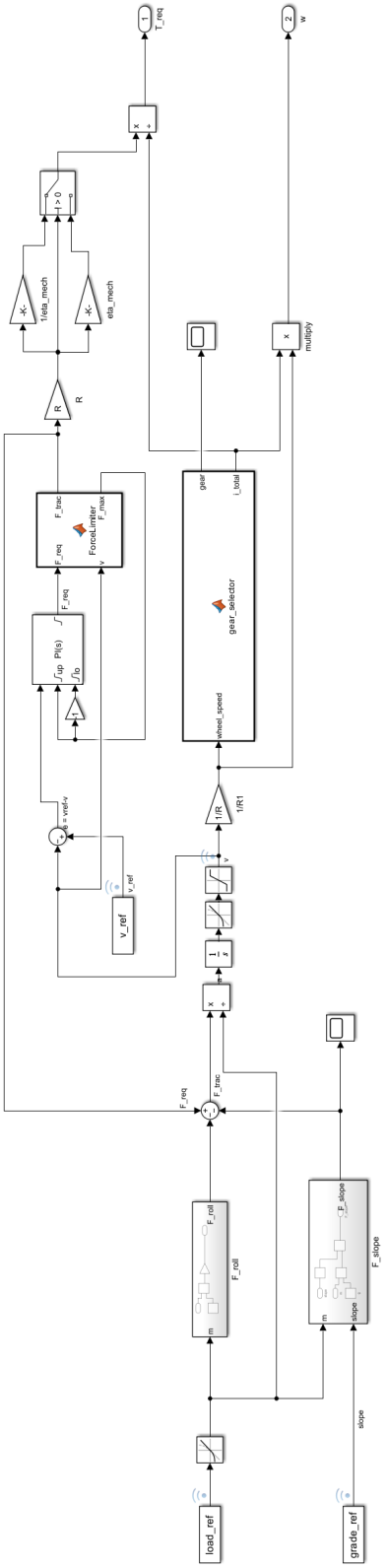

Figure A.2: Model1 Vehicle Longitudinal Dynamics

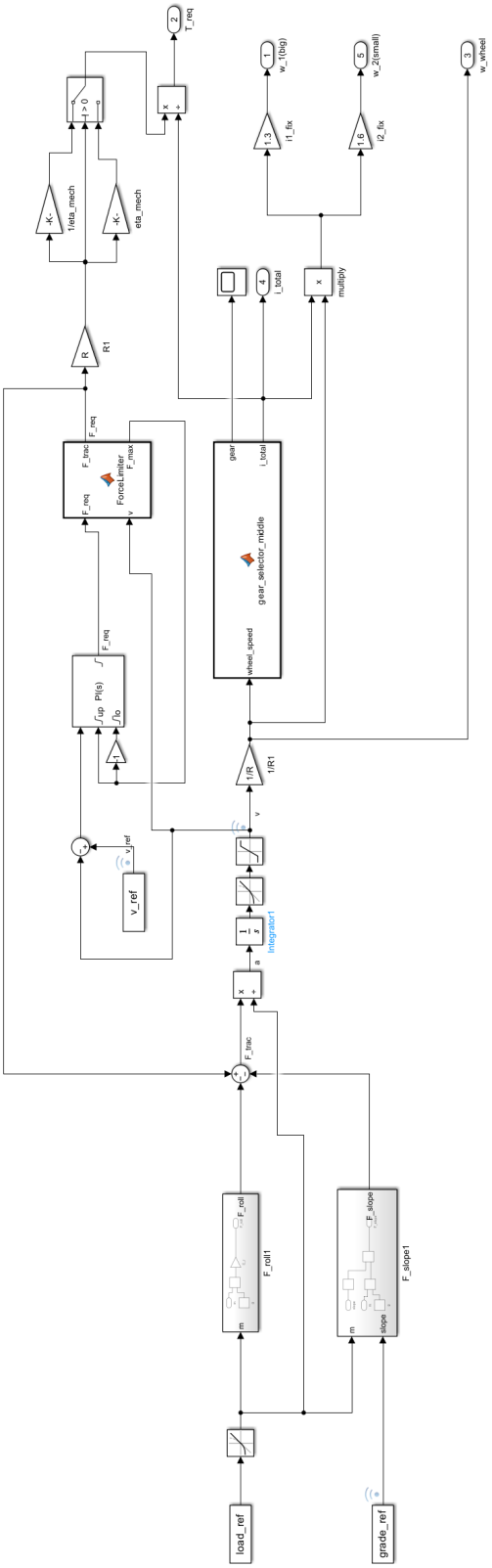

Figure A.3: Model2 Vehicle Longitudinal Dynamics

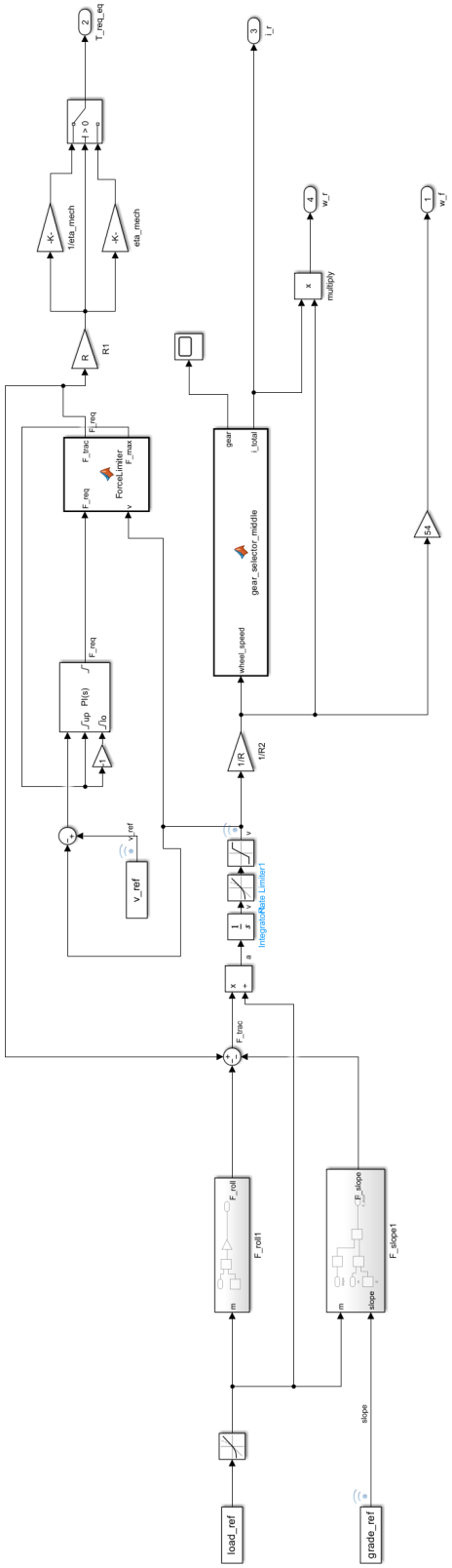

Figure A.4: Model3 Vehicle Longitudinal Dynamics

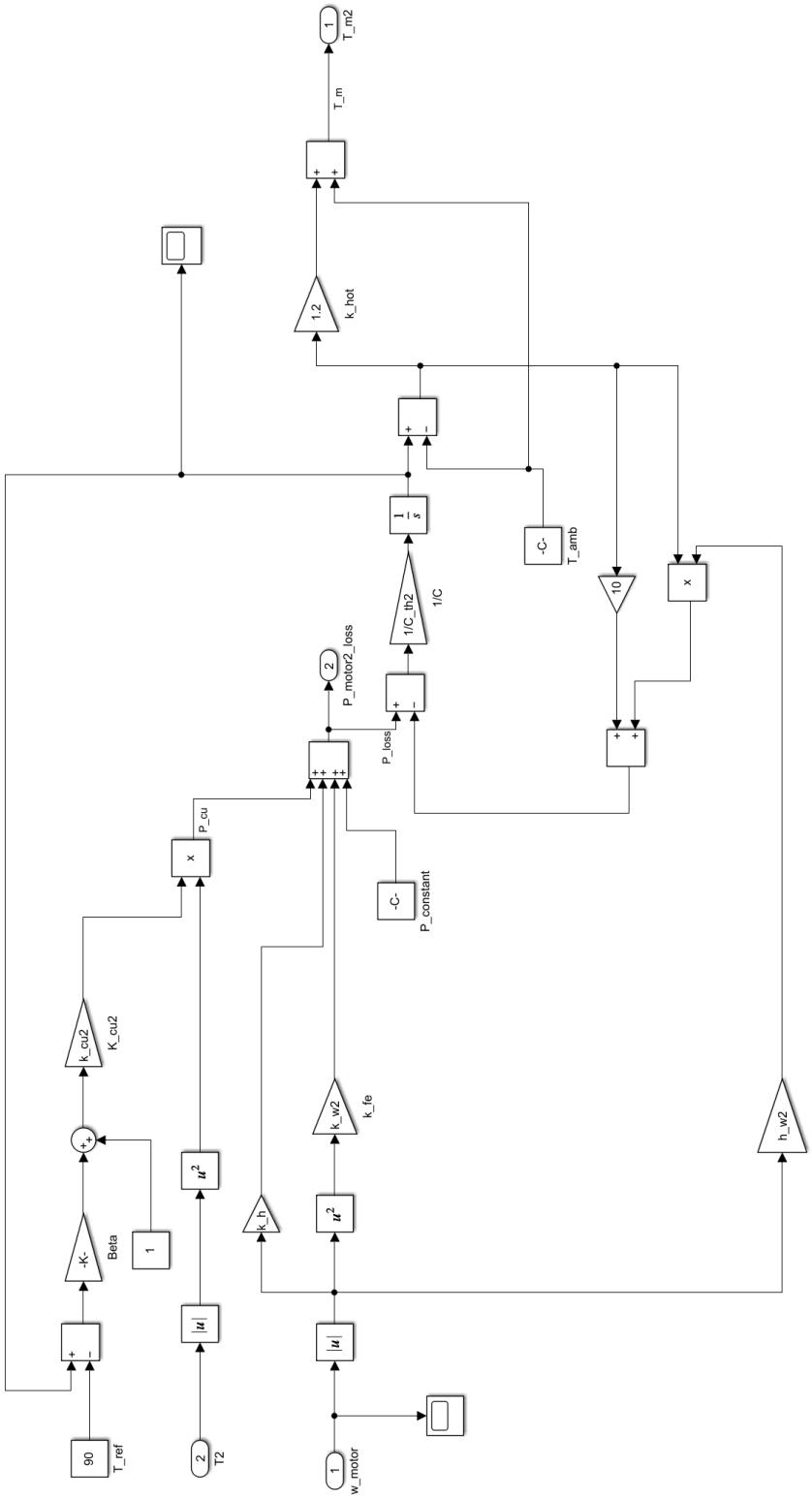

Figure A.5: Lumped-parameter thermal model structure

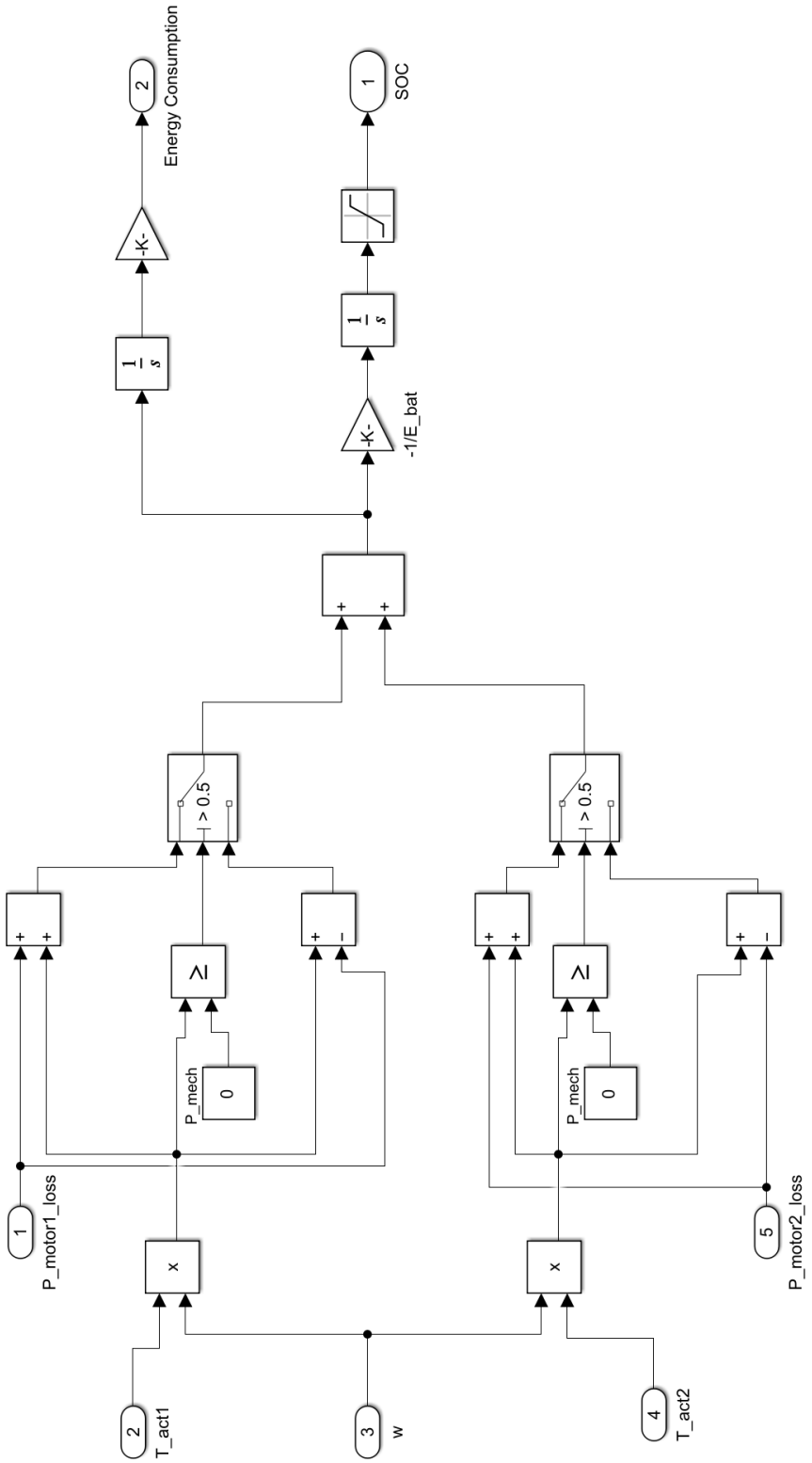

Figure A.6: Energy Accumulation Module

DEPARTMENT OF SOME SUBJECT OR TECHNOLOGY
CHALMERS UNIVERSITY OF TECHNOLOGY
Gothenburg, Sweden
www.chalmers.se

CHALMERS
UNIVERSITY OF TECHNOLOGY